



## Improve stiffening method on STIFF-FLOP based endoscope

G.R. (Gaston) Gabriël

BSc Report

**Committee:**

Dr.ir. H. Naghibi Beidokhti

Dr.ir. M. Abayazid

Dr.ir. J.F. Broenink

I. Khalil, MSc

April 2019

013RAM2019  
Robotics and Mechatronics  
EE-Math-CS  
University of Twente  
P.O. Box 217  
7500 AE Enschede  
The Netherlands



## **Abstract**

At times where flexible endoscopes are being used for surgery far away from the incision point, stability is often the lagging factor for a reliable control of the endoscope. Designs based on soft robotics can offer solutions to this problem. A design based on a soft robotic approach is the STIFF-FLOP, a cylindrical soft endoscopic module, consisting of three pneumatic chambers and one central lumen. The chambers can be pneumatically actuated, a positive pressure is applied to one or two chambers, the chamber increases in volume, resulting in a bend module. The main cylinder gets moulded with the soft material silicone. To be able to intervene surgically, adjustable stiffness of the module is necessary. A pneumatic controlled stiffening method, granular jamming, shows to be a possible solution, however it still has some flaws. Other stiffening methods are still open for discussion. Layer jamming is one of those methods, which is based on stiffening with friction between two contacting layers.

In this research a stiffening method based on layer jamming is implemented in a scale like design, in a novel approach. Actuation of the system induces interference from the adjacent scales. This contact will provide friction between the layers and thus will stiffen the construction. The scale friction counteracts possible external forces. Experiments are conducted to measure the amount of stiffening that this design/method can provide. It shows that the stiffening method applies stiffening only to a straight module, however quantification was not possible. Releasing the chamber pressure after max bend angle was achieved and stiffening method was applied, dropped the angle with 29.76%. To conclude, this novel design shows to apply stiffness to a straight module. More research is needed to find out if adjusting the scale size will improve the method such that it adds stiffness to a bended module.



## List of Figures

1	The use of rigid and flexible endoscopes for surgical procedures . . . . .	7
2	Multi-module STIFF-FLOP endoscope. Three modules with each three pneumatic chambers. Stiffening channel in central lumen. Pneumatic lines for actuating of the individual components. [1] . . . . .	8
3	Basic layer jamming principle. Positive pressure (P) decreases distance between sheets which results in friction. If force (F) stays constant, distance (L) will be smaller for greater P. [2] . . . . .	11
4	Snake like actuator . . . . .	11
5	Scale jamming on STIFF-FLOP module. Spring made from smaller section which have the edges on an angle in a scale pattern.[3] . . . . .	12
6	Mechanically activated layer jamming. Left: contracted state, small diameter, low stiffness. Right: extended state, small diameter, stiff. [4] . . . . .	12
7	Basics of layer jamming with the use of $n=1$ layer per overlap. On the left: STIFF-FLOP module with layers connected on top. On the right: actuated state of the method, membrane pushes down, flaps have contact and provide stiffening. . . . .	13
8	Overlap projection between two adjacent flaps. Increasing distance $arcdf$ and increasing bending angle $\varphi + \theta$ will result in a lower $P_o$ overlap. . . . .	14
9	Bending simulation for individual flaps with two different angles ( $\varphi$ ). Vacuum pressure induces force on top of the flap downwards and forces pulling down from the bottom. Legend shows amount of displacement. . . . .	14
10	Collision approach, two adjacent flaps. The set distance $df$ has an influence on the behaviour of $Q_i$ and the changing angles $\varphi_1$ and $\varphi_2$ . Horizontal blue line = straight module, curved = inner side bended module (current true side). . . . .	15
11	Results of amount of overlap between two adjacent flaps. High values are preferable. Results are plotted in a 3D plot with a 4 <sup>th</sup> dimensional colorbar. . . . .	18
12	Results amount of collision (negative) or no collision. . . . .	19
13	Unweighed product of overlap times collision. High values are preferable . . . . .	20
14	Weighed product of overlap times collision. Weighed factor of 2 on overlap. . . . .	20
15	Two versions of the STIFF-FLOP design. Braided external sheathing and braided internal sheathing . . . . .	21
16	Flaps connected with rings wrapped the STIFF-FLOP module. Membrane surrounds set up. Tubing for vacuum on top and for actuation of chambers on bottom. . . . .	22
17	Moulds for casting the part for the stiffening method . . . . .	24
18	Influence of flaps on bending angle actuated with different pressures. Small differences are measured. Lines are plotted with deviation. . . . .	25
19	Schematics of part assembly and the end product . . . . .	26
20	Setup and measurement for measuring the angle . . . . .	27
21	Setup and measurement for measuring the displacement . . . . .	28
22	Mean stair plot of changing angle due to chamber pressure increase and decrease, and actuation of the stiffening method. . . . .	29
23	Stair plot of changing angle due to chamber pressure increases and one release, for different vacuum pressures. . . . .	29
24	Vacuum displacement plot, with constant force. One case for non bended state, two cases with a bending actuated with 0.5 and 1.0 bar. . . . .	30
25	Force displacement curve of straight module, with and without applied stiffening. Only observational error is taken into account. . . . .	31
26	Technical drawing flaps . . . . .	35
27	Technical drawing membrane . . . . .	35
28	Technical drawing bottom piece . . . . .	35
29	Moulds for casting the parts of the design . . . . .	36
30	Different $df$ distances for experiment . . . . .	36
31	Force displacement curve with and without applied stiffening, for chamber pressure of 1.0 bar . . . . .	37

32	Frames from video of bending back experiment with 0.15 bar vacuum pressure stiffening actuation. . . . .	38
----	--	----

## List of Tables

1	Indicative variables for properties a variable stiffness endoscope has to have [5]	10
---	--	----

# Contents

<b>1</b>	<b>Introduction</b>	<b>7</b>
1.1	Soft robotics . . . . .	8
1.2	Research question . . . . .	9
<b>2</b>	<b>Literature research</b>	<b>10</b>
2.1	Stiffening methods . . . . .	10
2.2	Layer jamming . . . . .	12
<b>3</b>	<b>Modelling</b>	<b>13</b>
3.1	Principle . . . . .	13
3.1.1	Overlap . . . . .	14
3.1.2	Collision . . . . .	15
3.2	Mathematical model . . . . .	16
3.2.1	Overlap . . . . .	16
3.2.2	Collision . . . . .	17
3.3	Input selection . . . . .	17
3.4	Model analysis . . . . .	18
3.4.1	Overlap . . . . .	18
3.4.2	Collision . . . . .	19
3.4.3	Decision making . . . . .	19
<b>4</b>	<b>Design</b>	<b>21</b>
4.1	Design platform . . . . .	21
4.2	Principle . . . . .	21
4.3	Components . . . . .	22
4.3.1	Flaps . . . . .	22
4.3.2	Membrane . . . . .	22
4.3.3	Bottom piece . . . . .	22
4.4	Control . . . . .	23
<b>5</b>	<b>Fabrication</b>	<b>24</b>
5.1	Moulding . . . . .	24
5.2	Assembly . . . . .	25
<b>6</b>	<b>Experiments</b>	<b>27</b>
6.1	Testing set-up . . . . .	27
6.1.1	Bending back . . . . .	27
6.1.2	Force displacement . . . . .	28
6.2	Results . . . . .	28
6.2.1	Bending back . . . . .	28
6.2.2	Force displacement . . . . .	30
6.3	Experimental results discussion . . . . .	31
6.3.1	Bending back . . . . .	31
6.3.2	Force displacement . . . . .	32
<b>7</b>	<b>Discussion, Recommendation, and Conclusion</b>	<b>33</b>
7.1	Discussion and recommendation . . . . .	33
7.1.1	Model . . . . .	33
7.1.2	Design . . . . .	33
7.1.3	Fabrication . . . . .	33
7.1.4	Experiments . . . . .	34
7.2	Conclusion . . . . .	34

<b>8 Appendices</b>	<b>35</b>
8.1 Dimensions components . . . . .	35
8.2 Fabrication . . . . .	36
8.3 Experiments . . . . .	37
8.3.1 Notes experiment . . . . .	37
8.3.2 Force displacement on bended module . . . . .	37
8.3.3 Frames experiment bending back . . . . .	37

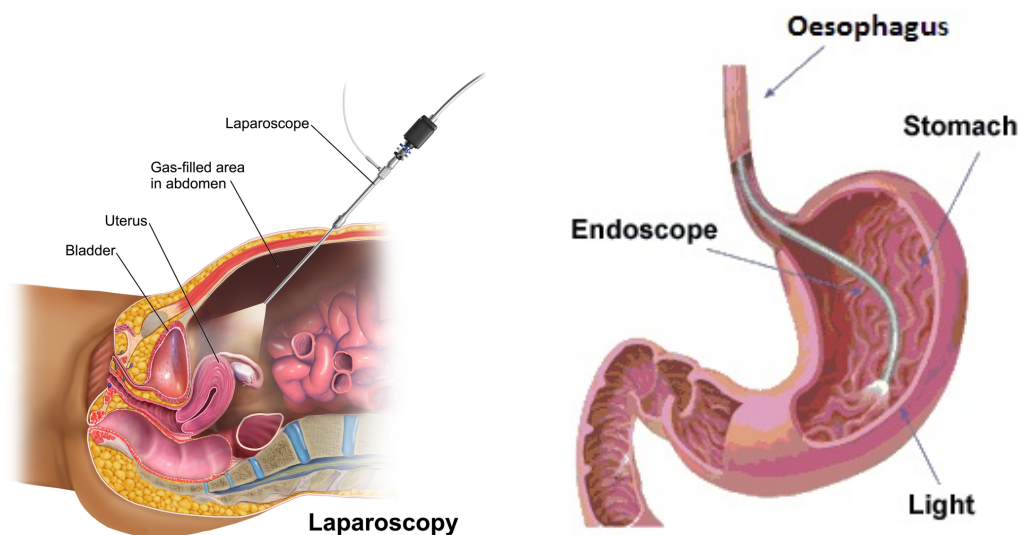
# 1 Introduction

Endoscopy is used to diagnose or operate at harder to reach sites in the human body. Invasive or minimal-invasive variants are used to enter the body with the endoscope to examine the body from the inside. Additionally, endoscopes are also used for interventions and direct treatment, biopsy can be taken, small tumours can be removed.

For examination close to the incision point, rigid endoscopes are used 1a. Here a laparoscope, a long fiber optic cable system, is used. With the use of this device, surgical acts can be performed at specific sites in the abdomen or pelvis area of the human body.

With the use of flexible endoscopes, areas farther away from the incision point are reachable. For examination of the digestive tract 1b, a flexible endoscope is inserted orally.

Due to the fact that rigid endoscope cannot bend, bypassing obstructions, such as organs and fragile tissue, is not possible. However, it gives high precision at the site of operation. At times where flexible endoscopes are being used for surgery far away from the incision point, stability is often the lagging factor for a reliable control of the endoscope. It is easy to comprehend that a flexible tube is not as well controllable as rigid ones. Whereas diagnostics can still be performed with this lag of stability, surgical intervention will not be possible. Furthermore, the flexible endoscope is difficult to track. When inserted, only the view from the camera gives a rough indication where it is positioned. The bends in these flexible endoscope are not well predictable enough. Also, the question whether the endoscope took the right turn at the intersection or not is way more difficult when a flexible endoscope for deeper targets is used. Not only the trackability at the intersection but also the controllability is often a problem. The surgeon can only control its movement from the tip of the endoscope. Even though the conventional instruments, are precise, well controllable, deliver stability, and can reach harder to reach places, a combination of the two is needed. A design combining the advantages of both rigid and flexible endoscope should be made. This could be achieved with the use of soft robotics.



(a) Laparoscopy: a rigid endoscope is inserted via an incision in the abdominal wall, the female reproductive system is examined. [6]

(b) Gastroscopy: a flexible endoscope gets inserted orally, examination of the gaster is possible. [7]

Figure 1: The use of rigid and flexible endoscopes for surgical procedures

## 1.1 Soft robotics

Soft robotics is a subfield of robotics, in which the material being used is highly compliant. Often, designs have taken inspiration from living organisms. The efficient designs of living organisms can offer interesting uses in robotics. Examples are: a robot fish [8], able to blend in the surroundings of the marine animals to explore the marine wildlife, and the Soft Robotic Glove [9], a portable, assistive, glove designed to augment hand rehabilitation for individuals with functional grasp pathologies. What may even be more interesting is the use of soft robotics for surgical applications.

In the last couple of years, several advances have been made in medical instruments that rely on soft robotics. One of which is STIFF-FLOP [10]: "A soft cylindrical module with three pneumatic chambers and one central lumen. Applying a positive pressure on a chamber will increase the volume and thus will apply forces within the chamber to bend the module." Stacking the modules on top of each other 2 results in a soft endoscope which is highly controllable, compliant, able to reach places far away the incision point, MR compatible and will be minimal to non-invasive. Endoscopic procedures will be fast, and thus more comfortable for the patient.

Besides the importance of actuation, the endoscope should be able to interact with the environment. With merely a soft endoscope the doctor cannot operate with high precision. Forces should also be absorbed by the endoscope, such that it will not bring problems to the trackability and controllability. A stiffening method has to be applied in order to bring stiffness to the endoscope when needed.

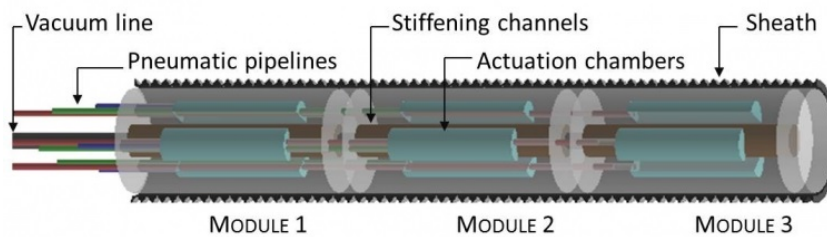


Figure 2: Multi-module STIFF-FLOP endoscope. Three modules with each three pneumatic chambers. Stiffening channel in central lumen. Pneumatic lines for actuating of the individual components. [1]

A variant of STIFF-FLOP, MOLLUSC manipulator [11][12], developed at RAM, has a stiffening method based on granular jamming. In addition to the fact that the chambers can control bending, they can control the stiffness. The stiffening channel has been removed from the STIFF-FLOP design and has been combined with the pneumatic chamber. Coffee-powder of a specific granular grind is placed in the pneumatic chamber to, when a vacuum is applied on the chamber, stiffen and resist a certain applied force. The adjustment of this STIFF-FLOP called MOLLUSC manipulator with granular jamming sac inserted, can mimic the stiffness level of the STIFF-FLOP but only with a couple of drawbacks. By applying the same pressure to the granular jamming sac, the air pushes the granules to the wall of the sac/wall of the chamber. The relatively stiff walls and the applied pressure will stiffen the coffee, resulting in a harder to bend module. Additionally, for a positive difference between the pressure and strength of wall material, the granules will often slip and/or coagulate at the bottom of the chamber. This stiffer construction will, while being pressurised with same pressure as without the sac, explode or rip the bottom apart. With the decreasing angle and major chances of rupturing, a solution has to be found.

## 1.2 Research question

To solve the problems current designs are having a research question is set up:

*"Which stiffening method is applicable on the STIFF-FLOP actuator such that it can provide adjustable stiffness and how would this be applied?"*

In order to optimise the process of this study, the next steps are taken:

More options to tackle the stiffening method problem are open for research. A small **literature** research on stiffening methods is done to orientate on the possible solutions. Applying the chosen stiffening method should also be done in a controlled way. A **model** is used to determine certain dimensions. The characteristics of **the design** are explained in detail. The design is fabricated and then tested with different **experiments**. Finally the results of those experiments are **discussed**.

## 2 Literature research

It is clear that choosing the right stiffening method is of great importance. It needs to provide the endoscope stiffness such that the doctor can treat with high precision. First, a couple of potential stiffening methods are going to be discussed. Afterwards, one of them is going to be selected. The selected stiffening method will be the base of the stiffening method used for this design.

### 2.1 Stiffening methods

Many stiffening methods are simply not suitable, because surgical requirements have to be taken into account. Table 1 shows the properties an endoscope has to have. Thus leading to a smaller selection to choose from. Three methods are chosen from the methods which are all compliant. Resulting in one final method which is going to be implemented in the module, so it can be tested.

Stiffness (Rigid State)	Stiffness (Flexible State)	Ultimate Force	Activation Time	External Diameter	Device Temperature
$\geq 330 \text{ Ncm}^2$	$\leq 165 \text{ Ncm}^2$	$\geq 16 \text{ N}$	<i>as small as possible</i>	$\leq 15 \text{ mm}$	$\leq 41^\circ\text{C}$

Table 1: Indicative variables for properties a variable stiffness endoscope has to have [5]

To begin with, granular jamming is a reliable stiffening method. It is fast and efficient, low cost, easy to manage, and very versatile [13]. Endoscopic modules such as STIFF-FLOP [10] and MOLLUSC [11] use this method because of those reasons. The method is based on the granular jamming of grains in a membrane. By applying a vacuum, the space between the grains will reduce and the grains will be in contact with each other, resulting in a rigid structure. Oppositely, releasing the vacuum and reducing the pressure difference between the pressure inside and outside the sac will make the sac more flexible. The grains have more freedom to move around, which will enhance the flexibility capabilities.

Both the grain properties and membrane properties are defining parameters. Grain size, surface condition, shape and material properties all have an optimal value to be the most sufficient for each use [14]. Different grain materials were tested, which were selected hypothetically. The study [15] showed coffee powder having a high strength-to-weight ratio in addition to large absolute strength. In the cases of STIFF-FLOP and its derivative designs coarse ground coffee powder is used. Further adjustments on this subject are still open for improvement.

Additionally the membrane is made of latex. The thin layer of latex will be made by dip moulding liquid latex into a balloon shape, in which the granular jamming material is inserted. The roughness of the membrane may have an influence on the locking properties of the grains to the wall of the membrane. This subject also needs further investigation [16]. Conclusively, current design can be improved without drastic design changes. When the overall effectiveness of the method increases, separate smaller channels for the granular jamming sacs can be made. This will result in a overall more effective smaller design.

Another method also based on structural mechanism is layer jamming. This concept basically relies on vacuuming space between two overlapping sheets to create friction, which results in a fixed position of the two sheets. This method can take on many forms, for example a snake like exterior for endoscopic applications [2]. This device is controlled via NiTi tendon wires, by pulling and extending the cables the robot can navigate past multiple obstacles. Stiffening can be achieved by applying a vacuum to the sleeve in which the snake layer jamming sheets are holstered, see figure 3 for basic method. This manipulator can be used for MIS or can eventually be combined with other stiffening methods.

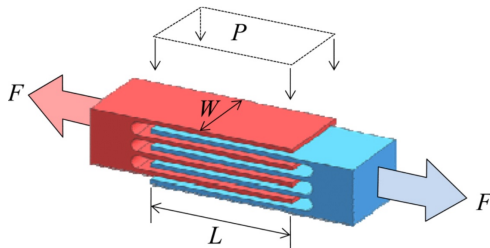


Figure 3: Basic layer jamming principle. Positive pressure ( $P$ ) decreases distance between sheets which results in friction. If force ( $F$ ) stays constant, distance ( $L$ ) will be smaller for greater  $P$ . [2]

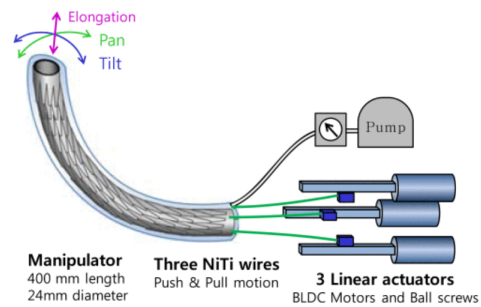


Figure 4: Snake like actuator

Electroactivate Polymers (EAP) are also a reliable method of stiffness control. This method is a more active approach of stiffening. In the case of Dielectric Polymers (DEP) is the speed of stiffening depending on the voltage amplifier. Applying a high order voltage between two electrodes will squeeze, in response to the Maxwell stress, the polymer, thus will make the polymer deform. The system being dependable on voltage flow, makes high speed of stiffening, whereas the destiffening speed is depending on the rate of discharge [17].

In the case of application, a soft robotic gripper [18] has been studied. A thin polymer made out of two electrode sheets is embedded with a specific pattern of fibers. These fibers will steer the direction of bending in a way such that the bending happens perpendicular to the fibers. Gripping actuators have been devised based on this technique. Small mass object can be gripped with these grippers.

Implementation in the endoscopic manipulators is, due to the MR compatibility restriction, not permitted. Smarter designs of more complex fiber patterns can be created for other disciplines in order to meet the requirements.

Each method has its own pros and cons. EAP's deliver fast and well controllable stiffness but are not MR compatible. Granular jamming is fast and delivers multivariate stiffness, though it requires to much room in the STIFF-FLOP design. Implementing the sacs in the pneumatic chambers brings more issues to the table. Optimisation of the technique can lead to a more efficient setup, though this study will not cover this option.

On the other hand, layer jamming has great potential for being the most suitable method. This method does not need to be in the module, it can be wrapped around the module, which will be beneficial for the fabrication and efficient use of space. A study [19] shows that it can stand up to large forces same as granular jamming.

## 2.2 Layer jamming

Several endoscope designs are already thought out with the use of layer jamming. Besides the snake like actuator [2], researched have combined scale like jamming in a helix form with the STIFF-FLOP design [3]. Jagged scales are placed on a helix backbone, a spring, in which the STIFF-FLOP module is situated, see figure 5. The scales will remain in contact with each other when bending is actuated. Cable tension as in catheter navigation system can increase the friction of the scales to stiffen the spring. Experiments show that this method has a higher deformation rate ( $\Delta x_e/l_{s0} = 0.428$ ) compared to the granular jamming by A. Jiang et al (= 0.25) and layer jamming by Kim et al (= 0.05). However this method shows a higher stiffness to device weight ratio, better wearability, and less hysteresis.



Figure 5: Scale jamming on STIFF-FLOP module. Spring made from smaller section which have the edges on an angle in a scale pattern.[3]

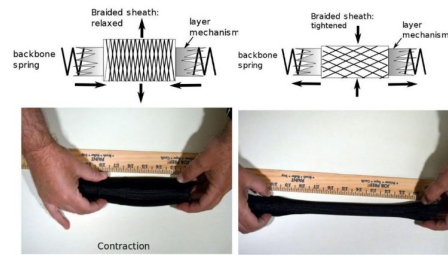


Figure 6: Mechanically activated layer jamming. Left: contracted state, small diameter, low stiffness. Right: extended state, small diameter, stiff. [4]

One more smart design using layer jamming has taken its idea from the dynamics of a kangaroos tail [4], see figure 6. When the marsupial is jumping around the tail is in compliant state whereas while boxing its tail is stiff and used as a third leg to stand on. Instead of using pneumatic actuation, a mechanical actuator in the shape of a spring is used to bring the flaps together to achieve stiffening. Flaps are revolved around a spring backbone which is encased by a braided mesh. This mechanically-woven mesh sheath will differ significantly in diameter when extended or compressed longitudinally, and is therefore able to apply pressure on the flap. As for every layer jamming based design, the more friction the more stiffening. This new actuated design performs comparable stiffness with even faster control. Besides, "it reduces the hysteresis, complexity, mass, and volume of the resulting overall system and additionally increases the reliability and portability for field applications." It shows to have a future in applications for robotic limbs and MIS.

### 3 Modelling

The selected stiffening method, layer jamming, cannot simply be applied to the module. The layers should have a specific shape and dimensions to be attached to the module. The design is going to be based on layer jamming with the use of flaps/scales. The chosen dimensions will have an influence on the effectiveness of the final design. To get a better understanding of what layer jamming, with the use of scales, is about, a 2D cross sectional drawing of one module (from 2) can be made, see figure 7. The sheathing is not included in this figure.

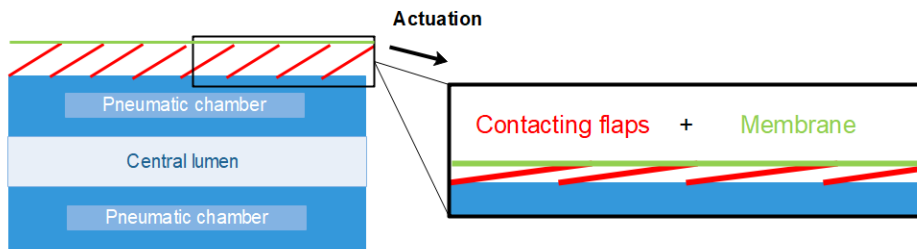


Figure 7: Basics of layer jamming with the use of  $n=1$  layer per overlap. On the left: STIFF-FLOP module with layers connected on top. On the right: actuated state of the method, membrane pushes down, flaps have contact and provide stiffening.

This simple figure showcases the foundation on which the method lies. In blue, the side wall of the endoscope, which will elongate and shorten due to bending. A membrane on top of the flaps will actuate the interference. After actuation the flaps will be in contact with each other and will induce frictional forces. From figure 3 we know that this mechanism induces stiffening. This simple figure will be used to determine the dimensions and thus characteristics of this stiffening method.

#### 3.1 Principle

Two main components are worked out in the model. First, the overlap of two adjacent flaps will be determined for different parameters. In the case of overlap there will be a contact area of friction after applying vacuum pressure. For different input values the overlap in 90 degrees bending is calculated. This set bending angle is to determine whether the overlap is still existent for a large bending angle.

Second, the amount of collision of the flaps in direction of bending, inner bending side, will be estimated. Higher amounts of collision will lead to higher forces needed to bend the module. In extreme cases, this will lead to a decrease in maximum bending angle and will increase the chances of ballooning and rupturing of the chamber.

### 3.1.1 Overlap

To begin with, characterisation of the overlap after actuation of the stiffening mechanism. Figure 8 shows the side view of two adjacent flaps. It is important to have in mind that in practice the surface area consists also of a width of the flap ( $w$ ). Though, this width is taken as a constant value for lowering the amount of inputs. On top of that, the overlap is only the the overlap between two adjacent flaps, however the total overlap between all the flaps will showcase a more realistic approach of stiffening, also this is not taken into account. On the other hand, this approach is able to compare the input values to eventually select the best parameters for the design.

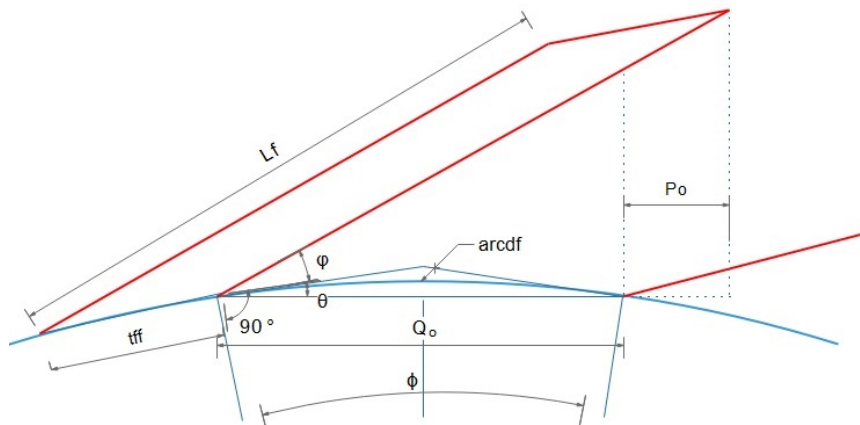


Figure 8: Overlap projection between two adjacent flaps. Increasing distance  $arcdf$  and increasing bending angle  $\varphi + \theta$  will result in a lower  $P_o$  overlap.

The blue line represents the outside of the module. The constant thickness of the strap is neglected. Without bending actuation,  $arcdf$  is equal to the set distance between each adjacent flap  $df$ . It changes shape due to bending and elongation. For a 90 degrees bending state the new distance and curvature can be calculated by adding the elongation between the two flaps to  $df$ . The angle between the flaps  $\Phi$  can be derived from this length. Geometry shows that  $\theta$  is equal to  $\frac{\Phi}{2}$ . Followed by an easy subtraction, gives  $P_o$ . The surface area after vacuum pressure should be approached with  $P_o$  as best as possible. Multiple assumptions were considered to best characterise the effect of the membrane and vacuum pressure on the bending of the flap. A simulation for bending of a single flap is done in order to optimise the accuracy of the actual dimensions of  $P_o$ .

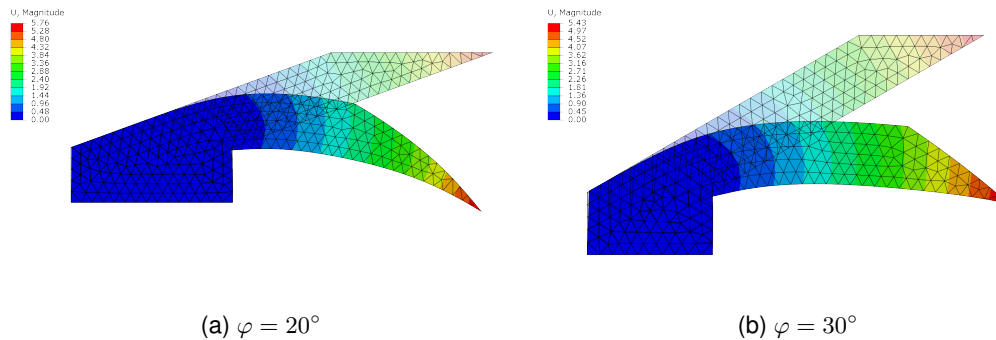


Figure 9: Bending simulation for individual flaps with two different angles ( $\varphi$ ). Vacuum pressure induces force on top of the flap downwards and forces pulling down from the bottom. Legend shows amount of displacement.

For two different flap angles ( $\varphi$ ) the effect of the membrane and vacuum pressure is simulated. Forces, pushing down the flap from on top (membrane), and pulling down the flap from below (vacuum), are applied. The flaps show a 92% and 96% true pure rotation for  $\varphi = 20^\circ$  and  $\varphi = 30^\circ$ , respectively. This validates the assumption of the pure rotation of the flaps and thus the approach of overlap  $P_o$ .

Additionally, the underside of the flaps are slightly elongated in positive x-direction. Looking at the displacement ( $U$ ), this  $P_o$  approach seems closest. This approach is only true for input of the selected range between  $\varphi = 20^\circ - 30^\circ$ . Higher values for  $\varphi$  are, due to the larger diameter, not used. The influence of  $\varphi$  will later be discussed in section 3.4.

Conclusively, the overlap is chosen to be a projection perpendicular to the line  $Q$  of  $L_f$  of the left flap to the topside of the right flap.

### 3.1.2 Collision

A decrease in bending angle for the same amount of applied pressure is undesired. Several influences can increase this phenomena. In general, adding mass to the module will make the actuation less: for the same pressure, more mass should be displaced, which makes the actuation less effective. On top of that, the flaps on the shortening side in bending can have an effect on the amount of bending. Shortening of the inner sides will make the flaps interfere, and will induce unwanted stiffening. The term collision is used to describe this effect.

A value for collision is approached by looking at figure 8 and deriving this one. In this model, two phenomena contribute to this effect: a decreasing  $arcd\theta$  and changing  $\varphi$  for both the flaps with respect to the straight module. The horizontal blue line represents the normal line, or straight module. The curved blue line is the actual wall of the module. Figure 10 shows the changing geometry after bending for two adjacent flaps.

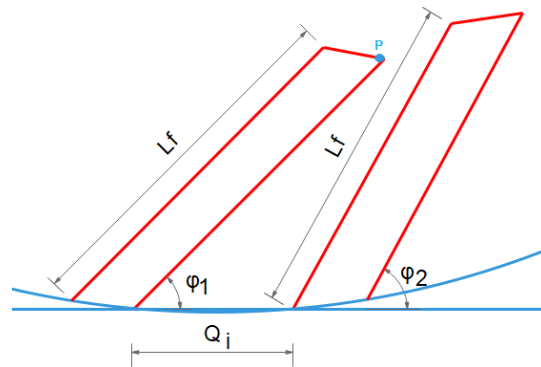


Figure 10: Collision approach, two adjacent flaps. The set distance  $df$  has an influence on the behaviour of  $Q_i$  and the changing angles  $\varphi_1$  and  $\varphi_2$ . Horizontal blue line = straight module, curved = inner side bended module (current true side).

The amount of collision ( $coll$ ) is a vector from point  $P$  to the intersection of the flaps when they do have a set length. A positive value means  $P$  is on the left side of the intersection of the lines, thus no collision for the actual length of the flaps. A negative value means that the point of intersection is located within the boundaries of the dimensions of the flaps, thus collision occurs. Variable  $Q_i$  is determined the same way as in subsection 3.1.1. Angles  $\varphi_1$  and  $\varphi_2$  are related with the angle  $\Phi$ , therefore with  $\theta$ , where  $\varphi_1 = \varphi + \theta$  and  $\varphi_2 = \varphi - \theta$ . These variables are used in equations (3.2) to determine the point of intersection, likewise the collision. In the end, a high value for  $coll$  is preferable over a lower one.

### 3.2 Mathematical model

To further go in detail on the actual steps the model makes to determine both  $P_o$  as *coll*, the equations are explained. First the movement of the endoscope has to be defined. The module has two degrees of freedom, which means that it is able to bend along two axes. The model is based on a set bending angle of  $90^\circ$  in a irrelevant direction. Elongation and shortening for pure bending can easily be calculated. Only the elongation is taken into these calculations, the steps for calculating the shortening of the inner side should be subtracted instead of summed. First the angle radius for the central line of the module has to be calculated, see 1.

$$2\pi r = L_{module} * \frac{360}{\theta_{bending}} \rightarrow r_{bending} = \frac{90}{\pi} \quad (1)$$

$$r_o = r_{bending} + \frac{d}{2} = \frac{90}{\pi} + 12.5$$

Next the length of the elongated side:

$$L_o = \frac{2\pi r_o}{\left(\frac{360}{\theta_{bending}}\right)} = 64.64mm \quad (2)$$

Which makes the total elongation on the outer side:

$$\Delta L_o = L_o - L = 64.64 - 45 = 19.63mm \quad (3)$$

The type of bending can be characterised as follows. Pressurising one of the chambers will put forces, when internal sheeting is applied, only on top and bottom of the chambers. Equation 4 tells us that higher pressure results in higher forces in a linear relation. The cross sectional area  $A$  stays the same, because diameter is constricted.

$$p = \frac{F}{A} \quad (4)$$

Adding the Euler-Bernoulli formula and Hookes Law [20] results in a elongation between two points formula:

$$\Delta dl = \frac{F_p}{AE} dl \quad (5)$$

With  $E$  for Young's Modulus of material. The total amount of elongation can be calculated when equation 5 is integrated over the length of the module. However this module assumes that the chamber will have the same length as the module, which is not the case. For the sake of simplification, the elongation will also take place at both bottom and top where the pneumatic chamber is not present. Dividing the total elongation over the length of the module gives an equation to determine the changed length between two points due to elongation. Where variable  $x$  is the distance between two points, which is, in the case of this model, *dff*:

$$\Delta L_{elongation} = 0.4362x \quad (6)$$

#### 3.2.1 Overlap

The overlap ( $P_o$ ) between two adjacent flaps do need to be calculated. Looking at figure 8, equation 6 can be used to determine the increasing *arcdff*, see section 3.1.1. The new distance between flaps *arcdff* can be calculated by simply adding up the elongation length. The new angle ( $\varphi_N = \varphi + \theta$ ) of the left flap can be calculated as follows:

$$\theta = \frac{arcdff * 90}{\pi * r_o} \rightarrow \varphi_N = \varphi + \theta \quad (7)$$

Which gives the final equation for determining the overlap ( $P_o$ ):

$$P_o = L_f * \cos(\varphi_N) - (2 * r_o * \sin(\theta)) \quad (8)$$

### 3.2.2 Collision

To calculate the *coll* vector, first the coordinates from the point of intersection need to be solved. Variables like  $Q_1$  and  $\varphi$  are calculated in the same way as above, but with negative 6 and subtraction of  $\frac{d}{2}$  in equation 1. For  $y_{in}$ -coordinates:

$$\frac{y_{in}}{\tan(\varphi_1)} = \frac{y_{in} + Q_1 * \tan(\varphi_2)}{\tan(\varphi_2)} \quad (9)$$

For  $x_{in}$ -coordinates, fill in  $y_{in}$ -coordinate from above:

$$x_{in} = \frac{y}{\tan(\varphi_1)} \quad (10)$$

The vector from intersection coordinates to tip of the left flap, point  $P$ , is calculated as follows:

$$Coll = \sqrt{(y_{in} - L_f * \cos(\varphi_1))^2 + (x_{in} - L_f * \cos(\varphi_1))^2} \quad (11)$$

Note that, for negative outcome of the subtractions, *Coll* must be multiplied with -1. These cases show a collision between the flaps.

### 3.3 Input selection

It is important to not just use random input variables for the model. The input vectors have to be selected with some kind of argumentation. Several factors play a role in choosing which input to take.

First, for the use of soft materials like silicone, the fabrication limitations put some minimum size on several components of the design. The flaps should be extracted from the mould as a whole, practice shows that moulding small layer silicone and extracting that brings problems. Hereby, the real thickness for the flaps ( $t_f$ ) is set to  $2mm$  and taken as a constant input.

Second, the length of each flap is constricted in maximum length. Longer flaps will have a higher chance of buckling and creasing. On the contrary, a longer length will result in more surface area. The relation between critical force and length of the flaps is given by this equation derived from Euler's critical load:

$$F = \frac{\pi^2 EI}{(KL)^2} \quad (12)$$

The length is in inversely proportional relation with the critical force:  $\frac{1}{L^2}$ . On the other hand, higher length means more overlap, thus more friction. Additionally the thickness is directly proportional with the area moment of inertia ( $I$ ) from 12. Higher  $I$  will result in higher critical force, the flaps are less sensitive for buckling. Also, a higher cross-sectional area ( $A$ ) will lead to less stress ( $\sigma$ ) on the flaps, leading to less strain ( $\epsilon$ ) 13.

$$E = \frac{\sigma}{\epsilon} \text{ and } \sigma = \frac{F}{A} \rightarrow \epsilon = \frac{F}{EA} \quad (13)$$

Friction is the main point of interest in this design. Equation 14 for tension force shows a directly proportional relation between the importance of the surface area  $A = w * L$ , applied pressure  $p$ , amount of flaps  $n = 1$ , and friction coefficient  $\mu$ .

$$F = \mu npwL \quad (14)$$

The equation shows that for a larger contacting area the friction forces are the highest, meaning that a higher contact area will lead to a stiffer layer jamming. This contact area ( $Po$ ) should be increased as much as possible to remain positive in a bended state. Because of elongation on the outer side, vertical distance between each flap will increase, resulting in a smaller possible contacting area.

On the contrary, major stiffening while bending is being actuated is not acceptable. Contacting flaps on the inner side of the bended module will overlap and collide due to the decrease of distance between the flaps. This could be detrimental to the point that it will counter bending of the module even without stiffening actuation. Friction between these

flaps will occur even before the vacuum is applied. For the least amount of uncontrollable stiffening this inner collision has to be minimised. Taken all this into account, for the length of flap an input from  $0\text{mm}$  to  $10\text{mm}$  is selected.

Lastly, the distance between flaps  $df$  consist of the thickness of the flap on the endoscope  $t_{ff}$  and distance of space in between two flaps  $df_f$ . Where  $t_{ff}$  is taken as a constant value of  $4\text{mm}$  and  $df_f$  a minimum of  $0.2\text{mm}$ . Which makes the input range for  $df$  from  $4.2\text{mm}$  to  $10\text{mm}$ . For larger  $df$  values there is no overlap due to the size of  $L_f$ .

### 3.4 Model analysis

The model has to estimate the best dimensions to choose for the final design. With the input chosen in section 3.3 the model calculates both the overlap ( $P_o$ ) and the collision vector ( $coll$ ). The individual results are going to be discussed, followed by a decision making section in which the components are combined and compared.

#### 3.4.1 Overlap

To begin with, the amount of friction should be as high as possible in actuated state of the stiffening method. This is approached by looking at the 2D-overlap mentioned in section 3.1.1. Figure 11 shows the outcome of the calculations the model did.

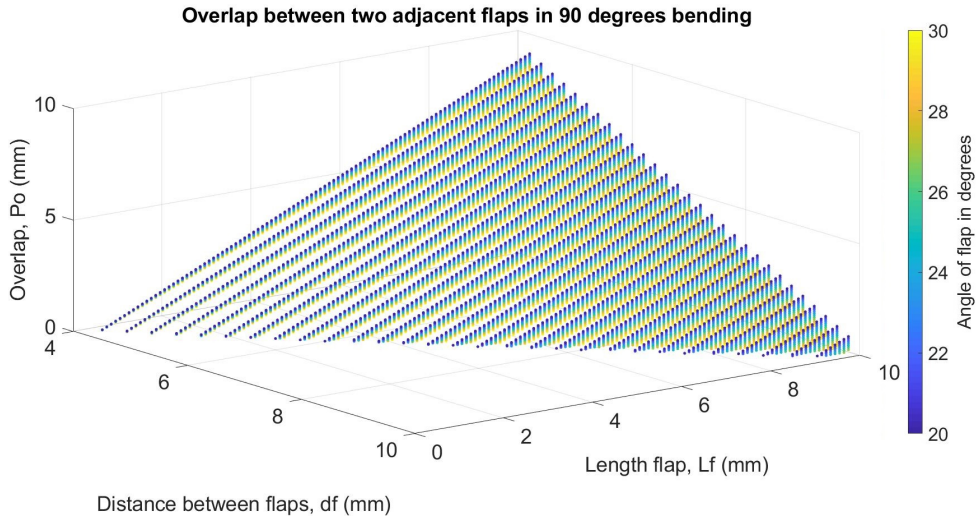


Figure 11: Results of amount of overlap between two adjacent flaps. High values are preferable. Results are plotted in a 3D plot with a 4<sup>th</sup> dimensional colorbar.

The linear increase of  $P_o$  is increasing with respect to both an increasing  $L_f$  and decreasing  $df$ .  $P_o$  values lower than zero are not shown here. The highest value for the angle  $\varphi$  is logically the best. Taking the highest value this plot gives and multiplying this with the width ( $w$ ) will give the estimated contacting surface area between two adjacent flaps. Only looking at this plot the selected dimensions of the flap are:  $L_f = 10\text{mm}$ ,  $df = 4.2\text{mm}$ ,  $\varphi = 30^\circ$ , with a  $P_o$  of  $9.098\text{mm}$ . The optimal point is hereby only limited by the input, not by the actual calculation. On the other hand, collision is also calculated.

### 3.4.2 Collision

The inner flap interference will also have an influence on the bending angle of the module. Figure 12 approaches that degree of stiffening for different flap dimensions.

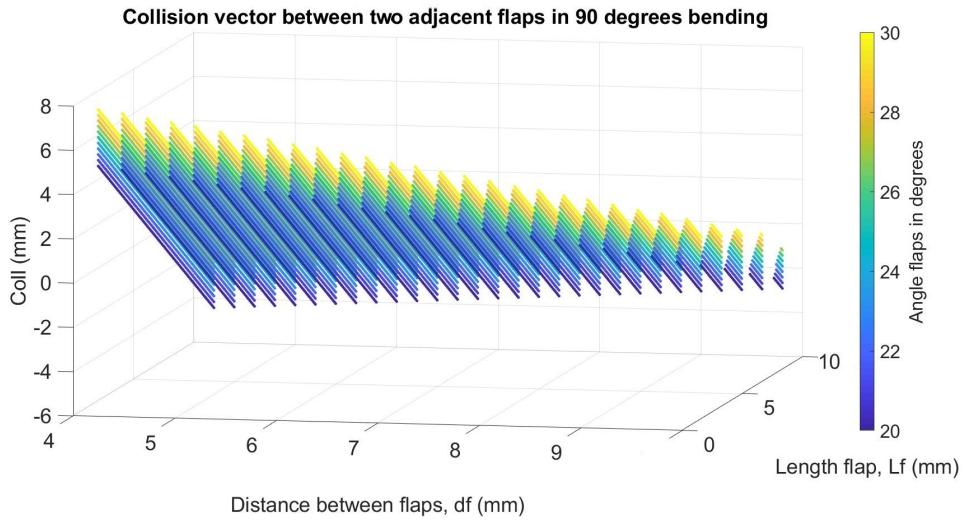


Figure 12: Results amount of collision (negative) or no collision.

Looking at the lowest points of the plot, it shows an increasing  $coll$  for larger  $df$ , which means that for increasing the distance between the flaps, the flaps are less likely to be in contact with each other. However a whole array of points are eliminated for  $P_o \leq 0$ , which makes the higher values having a small  $df$  size. Logically, smaller  $L_f$  show to have higher values. The most favourable dimensions with respect to the highest  $coll$  values are:  $L_f = 0.4mm, df = 4.2mm, \varphi = 30^\circ$ , with  $coll$  of  $7.723mm$ . However looking at  $P_o$  for these dimensions, it shows almost no existing overlap, which is not preferable. In order to select the best dimensions both results should be combined.

### 3.4.3 Decision making

For the dimensions where  $coll$  is the highest  $P_o$  is the lowest. To overcome this, the product of both the results is plotted. It is good to have in mind that this model does not tell anything about the minimum physical requirements for one of the results. Whether the  $P_o$  is more important than the  $coll$  is not modelled. However, it is of great importance that the main principle of the stiffening method, which is having the highest contacting surface area possible, is reached. This leads to two figures, one the unweighed product of the two results (13), and second the product of the results with a weight of 2x on the  $P_o$  (14).

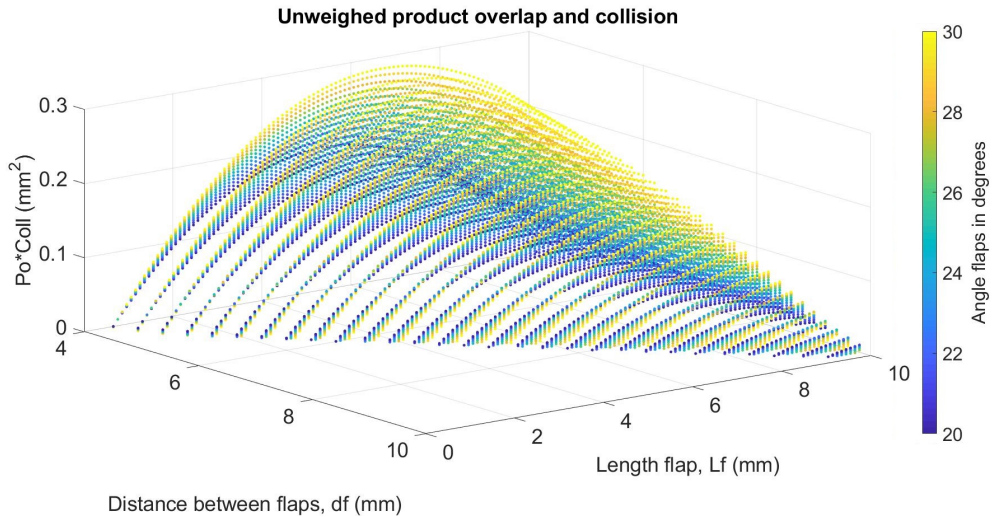


Figure 13: Unweighed product of overlap times collision. High values are preferable

Combining the two results shows a parabolic profile, with the area with highest value around:  $L_f = 4-8\text{mm}$ ,  $df = 4-6\text{mm}$ , and with maximum  $\varphi = 30^\circ$ . This area contains the points that are best considering both of the results  $P_o$  and  $coll$ , the values are relative to each other and will not be a indication of the actual amount of collision and overlap. Looking from a physical perspective, the two adjacent flaps in an  $90^\circ$  bending still show to have reasonable overlap between  $4-7\text{mm}$  with a collision vector value between  $4-0\text{mm}$ . Again, knowing that a high overlap is important for the stiffening method, a 2x weighed on the overlap is applied.

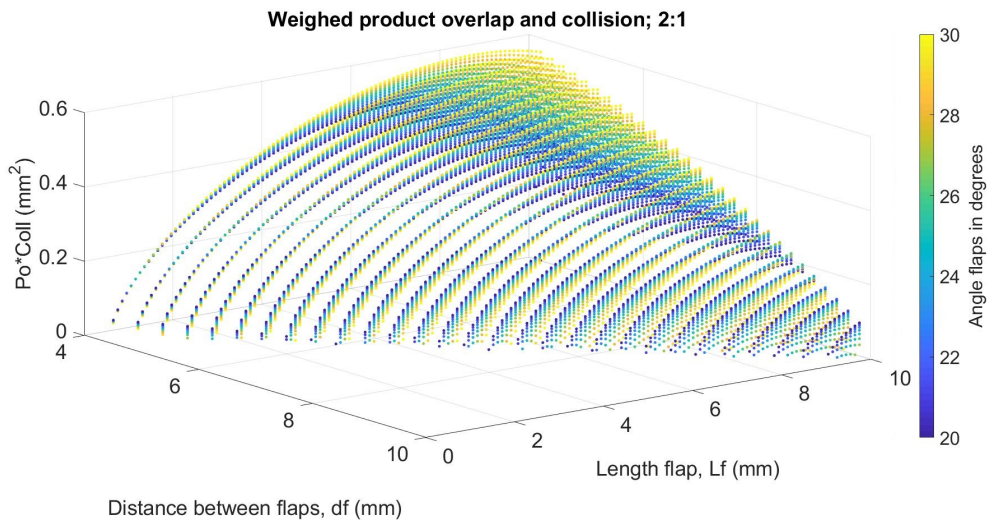


Figure 14: Weighed product of overlap times collision. Weighed factor of 2 on overlap.

The shape of the plot shifts more to the dimensions with larger  $L_f$ , which is obvious because in this area the overlap is the highest. Dimensions for the design are selected from this plot:  $L_f = 8.5\text{mm}$ ,  $df = 4.2\text{mm}$ ,  $\varphi = 30^\circ$ . The weighed of  $P_o$  can be increased, but it just moves the optimal values more towards the optimal values of figure 11. A minor influence of collision is still important, and factors such as buckling and strain do have to be taken into account 3.3.

## 4 Design

The design is based on the layer jamming principle and will be applied on the soft endoscope STIFF-FLOP. Actuation of the pneumatic chambers in the module will make the module bend. Stiffening mechanism can be applied to prevent the module from bending back and to apply more stiffness and strength to the module in actuated state. Layer jamming showed to have promising features and is therefore used in this design. The model already showed the main principle on which this design rests. The dimensions are selected and used to apply layer jamming on the module.

### 4.1 Design platform

The stiffening method is mounted on the STIFF-FLOP based module. Already discussed, the silicone moulded cylinder has three cylindrical spaced pneumatic chambers and one central lumen for tool housing. Figure 15a shows dimensions of each part. The stiffening channel is not used and remains empty.

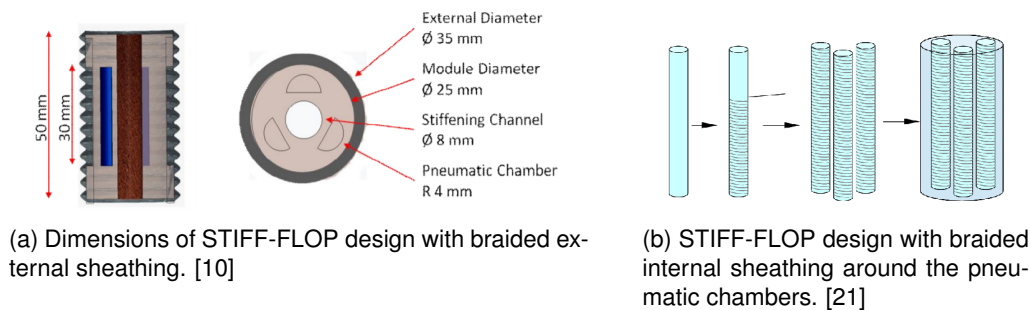


Figure 15: Two versions of the STIFF-FLOP design. Braided external sheathing and braided internal sheathing

This design uses external braided sheathing to limit the radial expansion, in order to maximise the elongation that bending induces. The forces pushing at the bottom and top of the chambers are the forces that induces the bending, these forces should be maximised. However with the use of a braided sheath, there will be less room for applying an external stiffening sleeve. Hereby, a STIFF-FLOP design with internal sheathing [21] is chosen. During the fabrication of the module, a thread is wrapped around each cylindrical chamber to constrain the chamber from radial increase as much as possible 15b. The chambers are also spaced in another way, such that, while activating two chambers simultaneously the angle would be the same as for one chamber actuation.

### 4.2 Principle

Brake like jamming layers cannot be simply applied to the endoscope because the endoscope will move in a 3D space, unlike the 2D brake like applications [22][19]. A design based on the snake like actuator has the biggest chance to deliver with the use of soft materials. Instead of film coated plastic, silicone is used. This design works on the same principle as the design mentioned, but with the use of only soft materials.

In this design (16) the scales from [2], are called flaps. The flaps are horizontally connected with rings and are vertically spaced on the endoscope. The module, together with its flaps, is surrounded by a membrane. Flaps will provide stiffness based on layer jamming while a vacuum pressured is applied. The flaps are positioned in a way that they have overlap with the flaps below or above. The overlapping surfaces can be brought together when there is an external force put on the upper flap, which is in this case caused by an applied vacuum between the flaps and the membrane. This vacuum will also apply a pull force on the bottom side of the flap. Contact of the flaps will provide friction between the layers. All the flaps together will be a 'in-length-changeable-backbone' of the module. In other words: the dynamic 'backbone' would be able to prevent the module from bending back and will strengthen the

module even when the module is bend. Bending back happens because of compression forces on the inner side and tension forces on the outer side, which is in the case of pure bending. Pure bending is assumed to simplify and used for modelling.

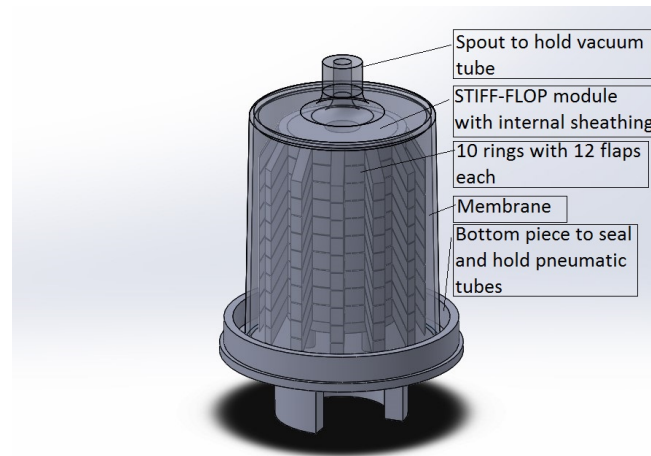


Figure 16: Flaps connected with rings wrapped the STIFF-FLOP module. Membrane surrounds set up. Tubing for vacuum on top and for actuation of chambers on bottom.

### 4.3 Components

The design is made up of several parts of which some dimensions are selected from the model. The flaps are placed on straps, the spacing and the amount of flaps use is explained. The membrane has to fit around the module with attached flaps, specific dimensions have to be selected. Last, the bottom part must house the tubing for actuating the chambers. It also should function as a platform on which the module is actuated. The dimensions of all the components are shown in appendix 8.1.

#### 4.3.1 Flaps

The flaps are parallelepiped shaped and made out of a silicone. With a width  $w$  of  $3mm$ , there are 12 flaps on each strap. The width is selected by looking at bending of a cylinder. The flaps perpendicular to the plane of bending also rotate with the bending angle, this induces the chance of collision between horizontal adjacent flaps. Flaps should not be too wide to have this effect cause any problems. The width is selected such that the horizontal distance between flaps is larger than, but almost equal as, its width. To maximise the surface area, the width is set to  $3mm$ , with a distance between flaps of  $\frac{\pi*d-3*12}{12} = 3.53mm$ . For  $d =$  diameter module.

#### 4.3.2 Membrane

For the use of the membrane, the wall thickness should not be too thick such that the wall becomes too stiff and will not wrap around the module while vacuum pressure is applied. Too small of a thickness and the walls becomes too vulnerable. A thickness of  $2mm$  is selected to deal with both aspects. On top, a  $4mm$  hole piece is created to inject the vacuum tube.

#### 4.3.3 Bottom piece

To get an airtight space, a bottom piece is included in the design. This piece will function as a some kind of mould in which the bottom layer of Ecoflex is poured, and as a platform which can be mounted on the standard, see 20a or 21a. It has three holes to fit the tubes from the pneumatic chambers through. The elevated border will hold the Ecoflex that is poured in to function as the soft seal.

#### **4.4 Control**

An app specially made for applying a controlled pressure is used to apply the vacuum pressure needed. This Matlab app includes controllability over the Arduino board. Initially, this app was designed to control the actuation of bending, thus applying a positive pressure into the pneumatic chambers. However this app is also able to control negative pressures. It sends out amount of voltage that the digital pressure regulator can translate to amount of pressure. The amount of vacuum is going to be tested and discussed in 6.

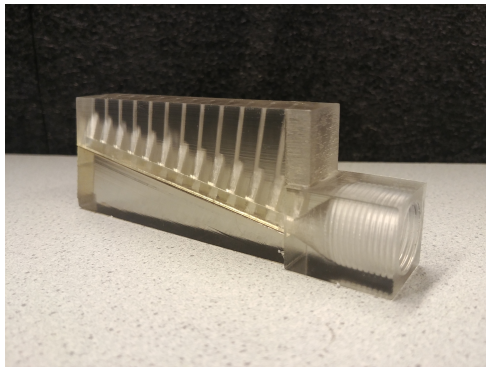
## 5 Fabrication

With the use of moulding technique two parts are fabricated. The bottom part is 3D-printed. Ecoflex from Smooth-On is the chosen silicone. This manufacturer makes a variety of different silicone with different strengths and elasticity's, also each variant has a specific pot life and cure time. With the knowledge of the material Ecoflex 50 is selected for both the membrane and flaps. After casting every part, the parts are assembled and the bottom piece is added. The first STIFF-FLOP with soft layer jamming is constructed.

After casting every part, the parts are connected with additional Ecoflex 30 to the module, after which the module will have its tubes through the 3D-printed bottom piece. A small layer of Ecoflex is poured in the bottom piece, the module is pulled down and the membrane is wrapped around the module such that the bottom of the membrane touches the liquid Ecoflex. Curing overnight will finish the assembly.

### 5.1 Moulding

The moulds 17 for the parts are 3D-printed in a high resolution printer, such that the surfaces are as smooth as possible, which makes extraction easier. A transparent polymer is used to easily track the silicone when injecting the moulds.



(a) Flap with straps mould



(b) Membrane mould, in upside down position

Figure 17: Moulds for casting the part for the stiffening method

A syringe filled with Ecoflex 50 is injected into the tapped hole. With small force the Ecoflex gets injected into the mould and flows from bottom to top through the mould. Eventually reaching the specially made air flow channels on the top. The silicone is first cured overnight, in the morning it is put in the oven at  $35^{\circ}C$  with multiple time intervals.

First the complete mould is put in the oven for 1 hour, followed by taking the part of that is not connected with the extrusion and placing it back in the oven for 2 hours. Finally, the silicone can be carefully peeled of the mould, to be followed by a cure in the oven at  $100^{\circ}C$ , to make sure that the material reaches its maximum strength. More figures are included in appendix 8.2

## 5.2 Assembly

All the parts have to be connected to become one whole piece made out of Ecoflex. For the distance  $df$  and amount of rings a small experiment is done, to give some kind of idea of the influence the dimensions have on the bending angle. The influence of the distance  $df$  on the bending angle is already mentioned in 3, however the weighed of the  $coll$  has not been characterised. For this experiment, the influence of different amount of rings and various  $df$ 's on the bending angle were tested 18. See appendix 8.2 for images.

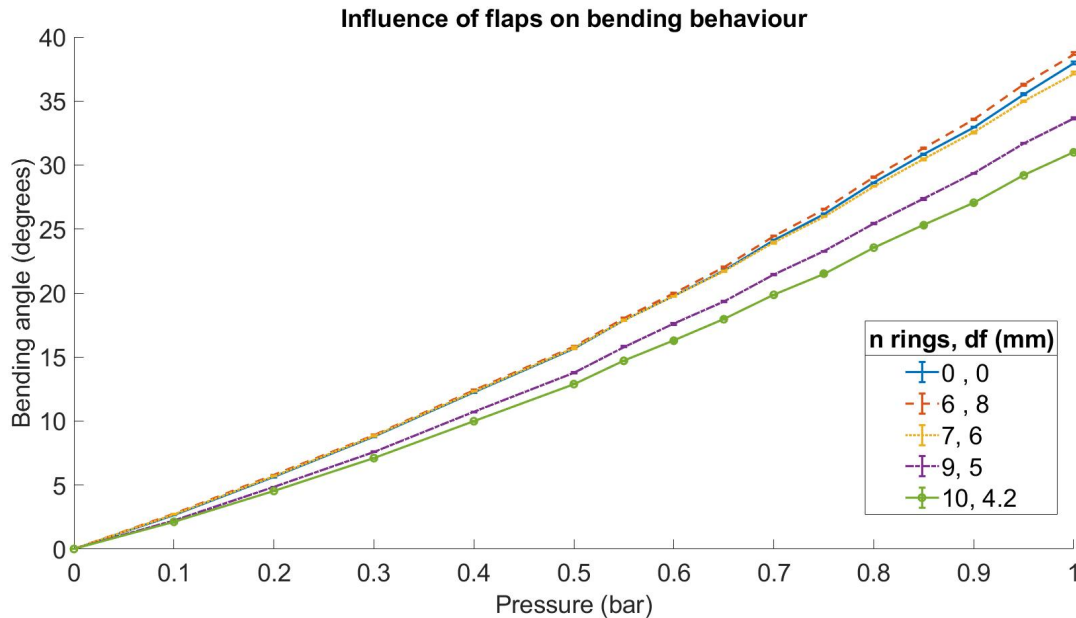


Figure 18: Influence of flaps on bending angle actuated with different pressures. Small differences are measured. Lines are plotted with deviation.

At low pressures the difference of bending is not that big, medium pressure, 0.4 bar, the difference becomes bigger. Eventually leading to a maximum difference between curve(6, 8) and curve(10, 4.2) of  $\Delta^\circ = 38.63^\circ - 30.99^\circ = 7.64^\circ$ , which makes is decreasing in angle by 19.78%. This decrease is as expected, because adding more flaps and decreasing the distance makes the flaps in bending state interfere, which will accumulate the stiffening. It should be noted that, in this set-up the rings were not fixed with Ecoflex to the module. Rings were only stretched around the module. A higher decrease could be noticed when attached with Ecoflex, because of adding more fixed material. On the contrary the amount of bending is still high enough such that experiments with bending and stiffening can be done. It is important to still use the overlap as the main point of focus. Conclusively, the decrease of bending, 19.79% is not of such high degree that a different  $df$  is selected, because choosing other dimensions will lead to less overlap. The selected dimensions from the model are going to be used for the final assembly.

The overall assembly takes place as follows. The steps are visualised in figure 19a.

**1**, each strap is shaped into a circle, so that it easily can be stretched around the module. Applying a small amount of Ecoflex on the distal ends of the straps will do the job. **2**, the parts are connected with additional Ecoflex 30 to the module. **3**, the tubes from the chambers get pulled through the holes of the bottom piece. A small layer of Ecoflex is poured in the bottom piece, the module is pulled down. **4**, the membrane is wrapped around the module such that the bottom of the membrane touches the liquid Ecoflex. A final cure overnight will finish the assembly 19b.

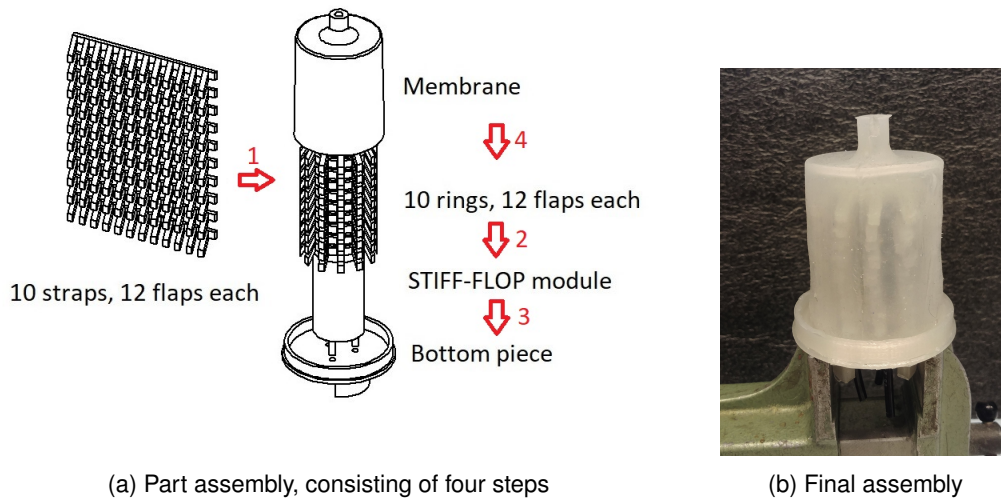


Figure 19: Schematics of part assembly and the end product

## 6 Experiments

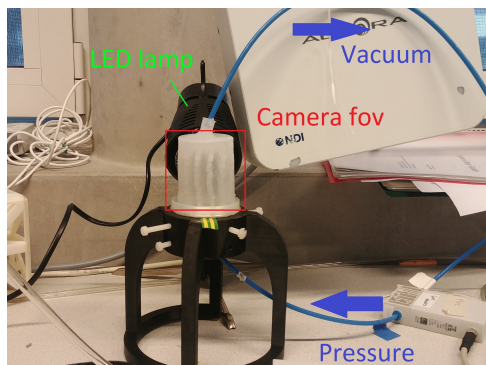
The STIFF-FLOP with stiffening method should have adjustable stiffness. Actuation of the stiffening mechanism should increase overall stiffness of the module. To prove the system works, two main experiments are conducted on the assembled components. First the bending back phenomena is tested. This will give an indication whether the stiffening method is able to deliver enough strength to counteract the tension and compression forces from the module that wants to bend back. Second the amount of stiffening will be tested in a force displacement experiment. The results are going to be discussed and in 7 a verdict is given. Some notes about the experiments are written out in appendix 8.3

### 6.1 Testing set-up

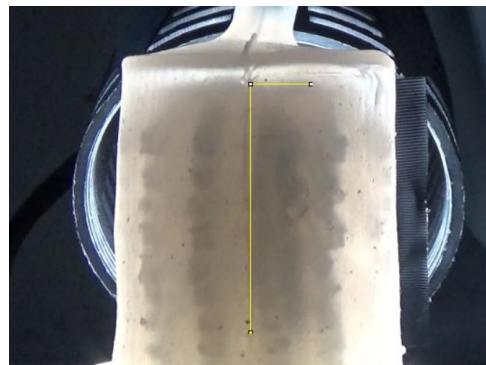
For each experiment a different experimental set-up is used. Measuring the changing angle for the first experiment is done with the use of a camera. The force displacement experiment is measured by marking the string used to apply force to the top of the module. Data of both experiments is collected and processed in the following sections. Matlab is used to process and analyse the data.

#### 6.1.1 Bending back

For normal actuation of bending the module will bend back instantly when chamber pressure is released. Forces that are put into the module by actuating it with air pressure want to compress and elongate the module in a counteracting manner. In the best case scenario, applying the stiffening method after the maximum bending angle is reached, and releasing the chamber pressure will fixate the angle. To track the angle during this sequence, setup 20a is used.



(a) Set-up used to track the influence of the stiffening method on the angle after pressure release



(b) Frame of video captured by camera used to measure angle with imageJ

Figure 20: Setup and measurement for measuring the angle

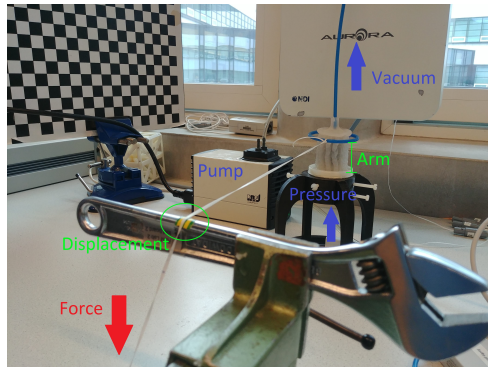
The module is placed on a standard to fit the tubing for the chamber. The chamber that actuates the bending to the right in the picture's plane is connected. The vacuum tube is connected and hung with a wire to minimise the hysteresis the mass of the tube brings. A LED lamp is turned on during the experiment, to increase the contrast of the contours of the module inside. Ambient lights are turned off during the experiment. Figure 20b shows the camera's field of view (fov). The angle between the top of the module and the vertical line is measured.

The experiment is divided in two parts. First part, sets of 3x2 experiments are done, the angle is tracked over time for with and without stiffening. The pressure is increased per 5 seconds with steps of 0.2 bar up to 1.0 bar. At 25 seconds the highest pressure is applied, without stiffening, the pressure is released. With stiffening, at 30 seconds vacuum pressure of 0.1 bar is applied, followed by chamber pressure release at 35 seconds. Finally, the vacuum pressure is released at 45 seconds. Every 2 seconds after a new input, the angle is

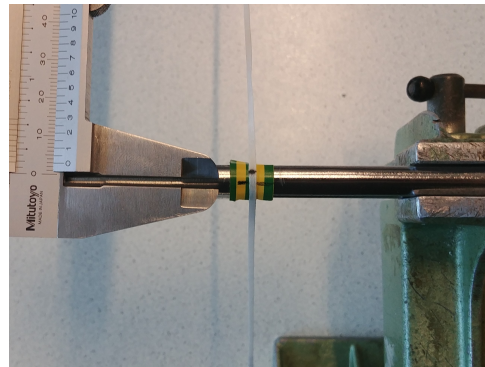
measured. For better understanding of the graph, the graph is shifted with 2 seconds to the left. Second part, experiment with the same time steps as first part but with varying applied vacuum pressures, without repetition.

### 6.1.2 Force displacement

To quantify the amount of stiffness, a force displacement experiment is used. Differences between non-vacuum displacement and vacuum displacement are going to be compared to measure the increased strength. Also strength that the actuation of the chamber accumulates is included, varying amount of chamber pressure are applied. Figure 21a shows the used setup.



(a) Set-up used to measure the displacement for a applied force.



(b) Measuring the displacement with a ruler. String should be aligned with 2<sup>nd</sup> green line.

Figure 21: Setup and measurement for measuring the displacement

A specific amount of weight is hung on the wire that is connected with the top of the module, which creates a momentum with  $arm = 45mm - 2mm(r_{bluetube}) = 43mm$ . Four weights are used in this experiment: 58 g, 166 g, 288 g, and 474 g. The wire is horizontally aligned and will be read out, after 3 seconds after releasing the weight, at the top of the tool 21b. The weight is used to apply the force. For the zero measurement, a clamp with a mass of 58 grams, is tied at the end of the wire, with moment of  $F * d = 0.058 * 9.81 * 0.043 = 0, 24Nm$ . A small line is drawn on the wire to set the zero point.

The first experiment is set up to check for correlation between the amount of stiffening with varying vacuum pressures. Vacuum pressures of 0 to 0.25 bar with steps of 0.05 were tested with a weight of 58 g. Also combination with chamber pressures of 0, 0.5, and 1.0 bar were tested. The second experiment tests on the actual relation between force and displacement for both the module with and without stiffening. All the weights are used and have been converted to force ( $F$ ). Also the displacement difference from actuating the bending is tested, which is included in appendix 8.3.

## 6.2 Results

The two experiments are divided in each two parts. First, the results of bending back are shown. One plot shows the difference between vacuum and no vacuum. The other plot shows the relation between amount of vacuum pressure and the angle. Second, the results of the force displacement are shown. One plot shows the displacement for different applied vacuums and chamber pressures. The other plot shows the relation between displacement, bending, vacuum pressure for two masses.

### 6.2.1 Bending back

For the bending back difference between no vacuum and vacuum, the chamber is released at **30s** and **35s** respectively. A stair plot 22 is used to get a better understanding of the idea of releasing chamber pressure. At the release of pressure, we call this angle drop, at **30s**

without stiffening, the angle goes instantly to  $0^\circ$ , straight position,  $\Delta^\circ = 0.80^\circ - 18.84^\circ = -18,04^\circ$ . The time that this takes is not measured, but is less than 2s 6.1.1.

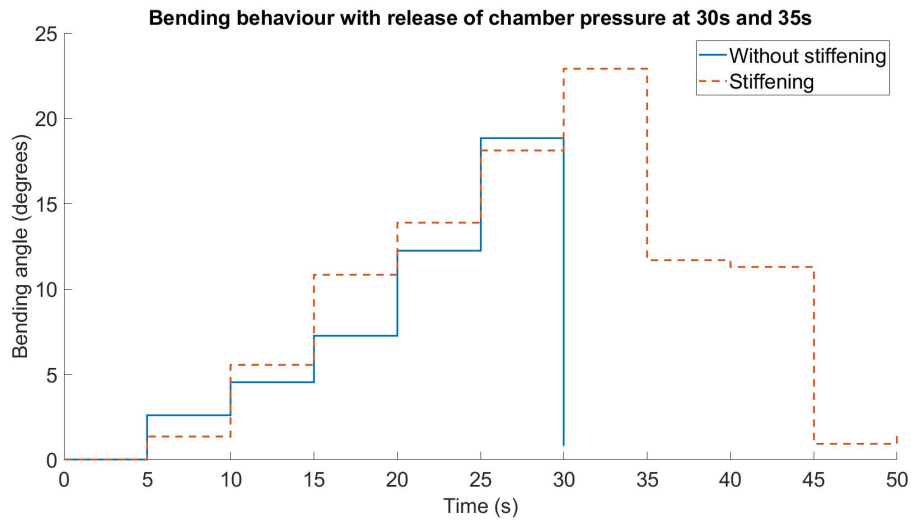


Figure 22: Mean stair plot of changing angle due to chamber pressure increase and decrease, and actuation of the stiffening method.

For using the stiffening method, at **30s**, vacuum pressure of 0.1 is applied. This lead to an increase of bending angle of  $\Delta^\circ = 22.9^\circ - 18.14^\circ = 4.76^\circ$ . At **35s** the pressure is released, the angle decreases with  $\Delta^\circ = 11.86^\circ - 22.9^\circ = -11,04^\circ$  or with respect to angle before actuation of stiffening method:  $\Delta^\circ = 11.86^\circ - 18.14^\circ = -6.28^\circ$ . A small decrease in angle is measured at **40s**. At last the vacuum is removed at **45s**, leading to a decrease to almost  $0^\circ$ .

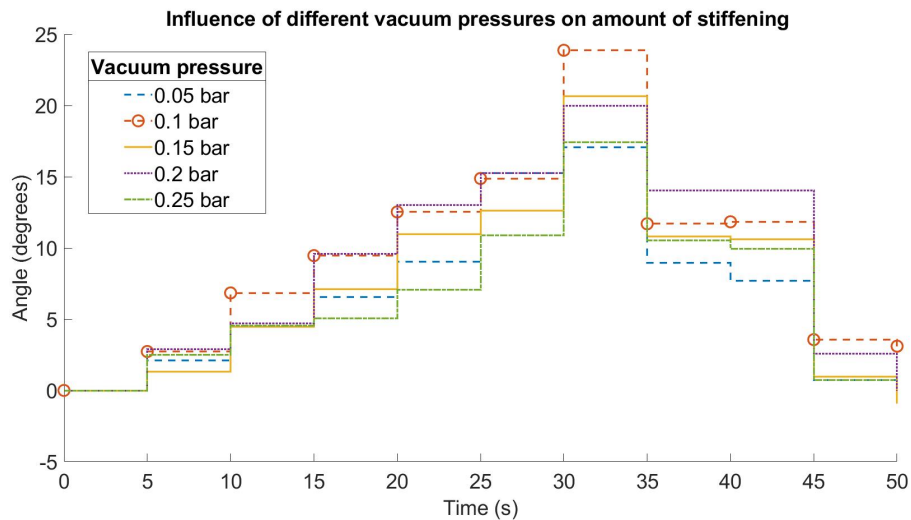


Figure 23: Stair plot of changing angle due to chamber pressure increases and one release, for different vacuum pressures.

The relation between the amount of vacuum pressure and angle decrease after chamber actuation is shown in figure 23. All vacuum pressures lead to an increase of bending angle, with the highest increase for 0.1 bar of  $\Delta^\circ = 9.00^\circ$ . For all applied vacuum pressures the bending angle did not drop straight to zero when chamber pressure was removed. Also the maximum difference of dropping angle between different vacuum pressures is  $\Delta^\circ = 6.23^\circ$ . The lowest dropping angle change is noticed for 0.2 bar of  $\Delta^\circ = -5.95^\circ$ , and with respect to before vacuum pressure, 0.25 bar of  $\Delta^\circ = -0.39^\circ$ .

In the period between **35s** and **40s** the vacuum is still applied, and for most of the cases

a small decrease in angle is noticed. It is striking that for a vacuum of 0.1 bar the highest increase after actuation is noticed and that the angle does not return to zero at **45s**. In appendix 8.3.3 a series of frames is shown from the measurement for bending back at 0.15 bar vacuum pressure.

## 6.2.2 Force displacement

Next, from the force displacement experiment two data plots are created. First, figure 24 shows the displacement after applying a weight of 58 g to the top of the module, in respect with the vacuum pressure. Numbers on vertical axis show a negative displacement difference with respect to 0 vacuum pressure per each different pneumatic pressure. Positive results show a stiffer module that displaces less due to the actuation of the stiffening method. Observational errorbar is created by measuring the displacement for one read out three times and taking the highest difference. For a vacuum pressure of 0.05 bar for module without bending, a  $3.5\text{mm}$  displacement is shown. A higher vacuum pressure showed only an increase of 0.1 and 0.2mm. However the error is higher than this actual increase.

When chamber pressure is applied, thus bending is actuated, the increase of displacement with respect to 0 vacuum pressure is not seen, because the error is higher than the fluctuations.

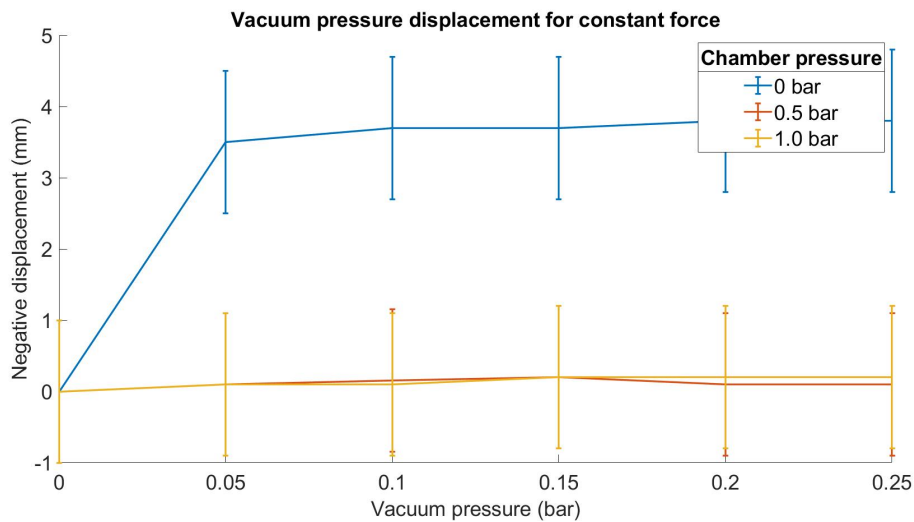


Figure 24: Vacuum displacement plot, with constant force. One case for non bended state, two cases with a bending actuated with 0.5 and 1.0 bar.

Second, plot 25 shows the displacement with respect to the force. The forces for each weight were calculated. A total of four different masses were used for the experiment. Both the curves show the difference between the zero measurement. In this plot, higher displacement values are not favourable.

At first sight, the 0 bar line shows to have a linear gradient with a notch at  $F = 2.8\text{N}$ . The line from 0.2 bar, stiffening method applied, shows to have almost a linear gradient without looking at the observational error. The lines between the first two forces are almost parallel,  $\Delta\text{mm}$  of  $3.8\text{mm}$  and  $3.7\text{mm}$ , followed by  $\Delta\text{mm}$  of  $1.4\text{mm}$  and  $6.6\text{mm}$ . It is possible to state that the amount of added force this direction can handle within this experiment lies between 1N and 2N, for the same amount of displacement.

The curves from the bending actuation are not shown because of a failure in the experiment, but are included in appendix 31 .

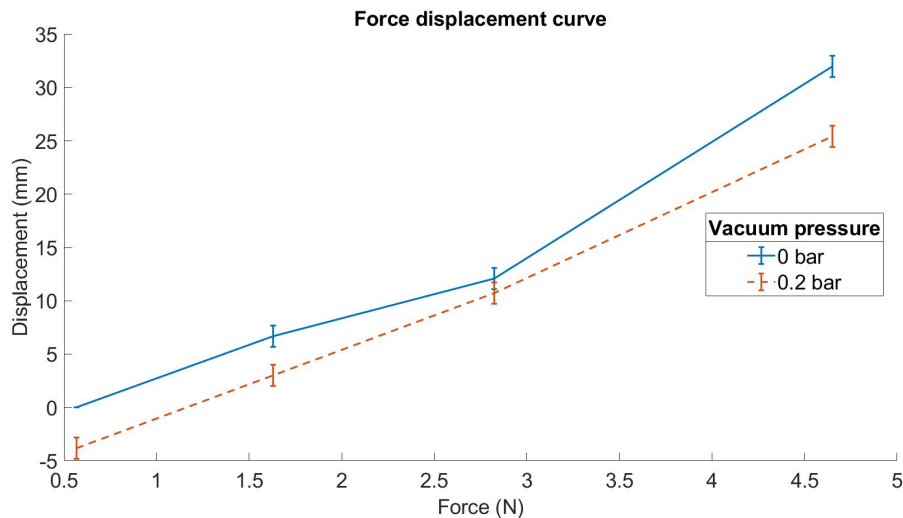


Figure 25: Force displacement curve of straight module, with and without applied stiffening. Only observational error is taken into account.

### 6.3 Experimental results discussion

First the discussion about the experiment that measured the bending back. Second the force displacement experiment is discussed.

#### 6.3.1 Bending back

To begin with, this experiment will not quantify the amount of stiffening, but will check if the method applies any counter forces when bending back. The stiffening method showed to decrease the amount of bending back by a maximum of  $5.95^\circ$  with the use of 0.2 bar. At the corresponding bending angle of  $14.04^\circ$  the overlap is high enough to induce enough friction to provide enough stiffening such that the bending back forces were balanced out.

It is important to remember that measuring the angles with imageJ is not precise, the observational error is  $3^\circ$ . Also the position of the components in the setup could have been off, leading to not measuring the actual bending angle. However these errors are not big enough to state if the stiffening method has an effect on bending back or not.

The increase of bending angle when vacuum pressure is applied, is for now not favourable, the characterisation of the bending becomes more difficult. The pressure from the membrane on the bended module may cause this increase: the surface area on the elongated side is bigger than the are on the shortened side, we know that  $F = p * A$ , meaning that for a bigger area there will be more force for the same amount of pressure. This leads to a higher force on the outer side which bends the module further.

In every repetition with other inputs the angle increase differently with respect to the chamber increasing pressure. To tackle this, the percentage of angle drop is taken with respect to the highest reached angle, this results in the least angle drop of 29.76% with 0.2 bar.

To conclude, from this experiment it can be stated that 0.2 bar vacuum pressure is best to have the lowest angle drop possible. To further check the optimal vacuum pressure the experiment should be done with more repetitions. Another technique, like an EM-tracker, should be used to measure the angle.

### 6.3.2 Force displacement

The first experiment 24 shows that when the chamber is pressurised the stiffening method does not deliver more strength to the module. Even for chamber pressure of 0.5 bar, with bending angle between  $5^\circ$  and  $10^\circ$  (22, 23) there is no added stiffening from the stiffening method. Several things can have caused this. The amount of overlap could be too little for this bending angle, the flaps may slide with respect to each other due to lack of friction. Additionally, when there is less overlap,  $L$  from 12 is higher, the chance of buckling increases. To further study this, smaller chamber pressures lower than 0.5 bar have to be tested, in order to test the stiffening method at lower angles. Also, the amount of overlap for a particular angle can be calculated from the model and coupled with this experiment.

The results from the second experiment show that the stiffening method clearly brings more stiffness to the system, but the quantity cannot be precisely determined from this experiment. Quantification of the stiffening could have been possible if a gradient for both with and without stiffening is found. Many uncertainties causes not be able to do this. The instability of some components in the set-up entails problems for measuring small changes in displacement. The degree of precision is important to characterise the gradient of each curve.

For the read out of the displacement a 3 seconds delay after releasing the weight was chosen. A better option would have been to measure the displacement after the summed up net forces were zero.

However, all this does not alter the fact that the stiffening method increased the strength of the straight module in its tested direction, and that it may be possible that the stiffening method, for smaller angles than approx  $6^\circ$ , can apply stiffening.

## 7 Discussion, Recommendation, and Conclusion

To conclude this research, discussion and recommendation is done. Followed by a conclusion. Each subject will be examined.

### 7.1 Discussion and recommendation

The paragraphs are divided in several subjects.

#### 7.1.1 Model

The model is used to give indicative dimensions for the design. The model neglected some phenomena for simplification purposes. Only two dimensional has been calculated for different input variables. Bending is not linear, experiments showed that the point of rotation is not parallel with the bottom of the module, also deformation of the top occurred when chamber pressure was applied. The decision making problem was only based on the overlap and collision, the weighed of each phenomena was guessed. However, the minimum amount of overlap is not estimated with the use of the mechanical mechanism on which the stiffening is based.

The model does have some uses. Combining the experiment results with the model can give a better idea of the minimum required amount of overlap for different bending angles. Hereby, the overlap is linked to the amount of stiffening for different bending angles. For further studies, finite element modelling can be used to optimise the decision making.

#### 7.1.2 Design

During the experiment, the design showed to function as expected. The membrane is air tight and is able to apply forces on the flaps. The flaps have overlap when the vacuum pressure is applied. But the amount of overlap showed to be too little when bending is actuated. Other flap shapes can be tried too increase the overlap and still minimise the interference with the horizontally aligned flaps when bending is actuated. This design can still be used to study the amount of overlap needed for stiffening with actuated bending.

#### 7.1.3 Fabrication

The stiffening method is completely made out of soft material, namely Ecoflex. Moulding techniques are used to get the best results. Curing of Ecoflex in small crannies showed to cause difficulties. Instructions call for a minimum cure time of 4 hours. The first extractions were done after one overnight cure, they resulted in a sticky not cured silicone. This is fixed by curing in steps, already described in 5.1. This did lead to a long fabrication progress, which was for this study's length critical.

Besides, the experiment for determining the influence of the flaps on the amount of bending was not that good of a representation of the final prototype. When Ecoflex was used to fixate the rings to the module, a small amount ended between the rings, which glued the rings all together. This increased the diameter of the module, which lead to a decrease of max bending angle between  $7^\circ$  and  $14^\circ$ .

To solve the low stiffening increase, silicone with higher E-modulus can be used to increase the critical force for buckling, and will lead to less strain of the stacked flaps when they need to function as a stiff 'dynamic' backbone 13. Also the area moment of inertia ( $I$ ) can be increased by increasing the width of the flap ( $w$ ), this also helps with reducing the amount of strain 13.

#### 7.1.4 Experiments

Experiments were done to test the stiffening method. One experiment was used to test if the stiffening method can hold the module in its place after releasing from a bend position. One test showed a decrease in angle of  $5.95^\circ$ , equal to 29.76% of its previous angle. The different angles of the individual tests makes it more difficult to compare the results. More repetitions have to be done in order to characterise this effect.

The experiment showed that the stiffening method does not apply strength to the module when 0.5 bar or higher is applied to one chamber to actuate the bending. For this linked bending angle the flaps are not able to provide stiffening, they have to little overlap or the length of the flaps, that is sensitive for buckling, becomes too large. Also the used material may show too much strain when a force is applied.

It is important to know that, only one direction of stiffening, force application site, was tested. Realistically forces can come from every other direction, these directions should also be tested.

More precise measure instruments such as a EM-tracker should be used to small changes in angle and linear displacement. In the best case scenario the whole central lumen is tracked in every experiment, in order to really characterise the influence of the stiffening method.

## 7.2 Conclusion

In this study, layer jamming with a scale-like design is applied to the STIFF-FLOP actuator. A model is used to give indicative dimensions for the design. With the selected dimensions for the flaps and rings a design is made. Experiments are done to test whether the stiffening method delivers more stiffness for both a non bended module and a bended module. Stiffening method applied on the straight module showed to need between 1N and 2N more force for the same amount of displacement in the tested direction. Applying bending to the module with 0.5 bar pressure, it showed that the stiffening method did not add more stiffening to the system. This may be solved by increasing the length ( $L_f$ ) and or the width ( $w$ ) of the flaps. Future research has to be done to combine more repeated experiments with a finite element model, and will have to improve the optimal dimensions for the flaps.

In the end, STIFF-FLOP module with the soft layer jamming showed to have increased stiffness for a non bended state with the use of this design. The design has the possibilities, to apply stiffness to a bended module.



## 8 Appendices

### 8.1 Dimensions components

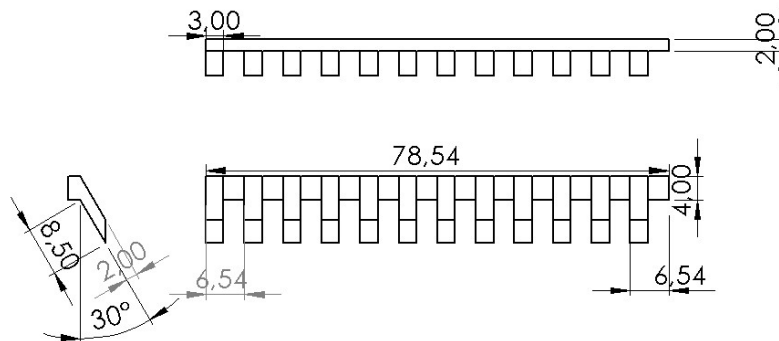


Figure 26: Technical drawing flaps

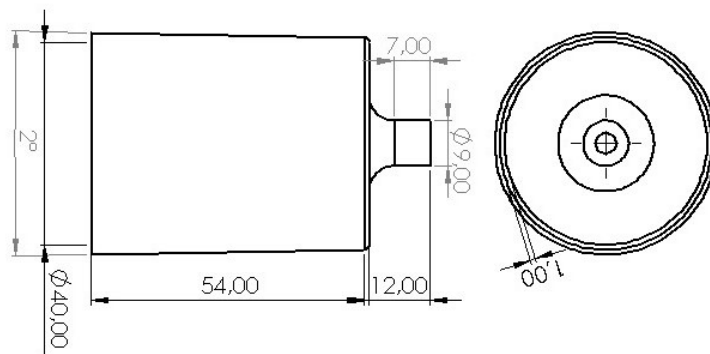


Figure 27: Technical drawing membrane

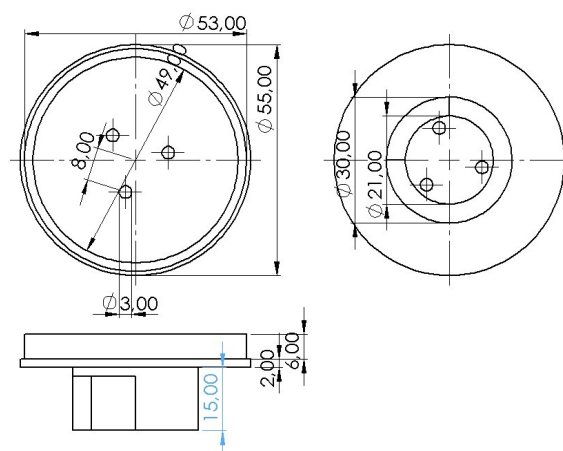
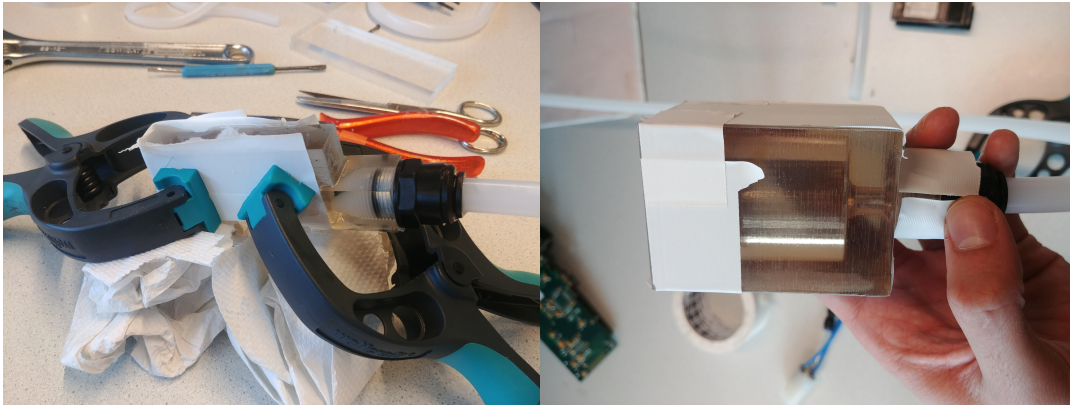


Figure 28: Technical drawing bottom piece

## 8.2 Fabrication

The mould parts are first sprayed with mould release spray, taped, then injected with a syringe.



(a) Flap with straps mould

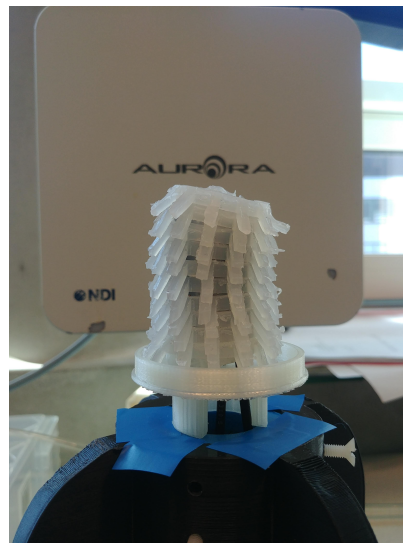
(b) Membrane mould

Figure 29: Moulds for casting the parts of the design

This experiment was done without the membrane. The rings had to be still changeable and movable.



(a)  $df = 8\text{mm}$



(b)  $df = 4.2\text{mm}$

Figure 30: Different  $df$  distances for experiment

## 8.3 Experiments

### 8.3.1 Notes experiment

After many actuations of both the chamber and the stiffening mechanism, now when vacuum pressure is applied, the top of the module shows a non cylindrical deformation. The top has an oval shape instead of the expected circle shape. The shortest diameter is in the direction of bending from the chamber that was used for all the experiments.

### 8.3.2 Force displacement on bended module

At the last test, with largest weight, the pneumatic chamber rupture and air flowing out was audible.

This plot 31 again shows that for a bended module the stiffening method was not able to provide more stiffening, in other words, less displacement for the same amount of force.

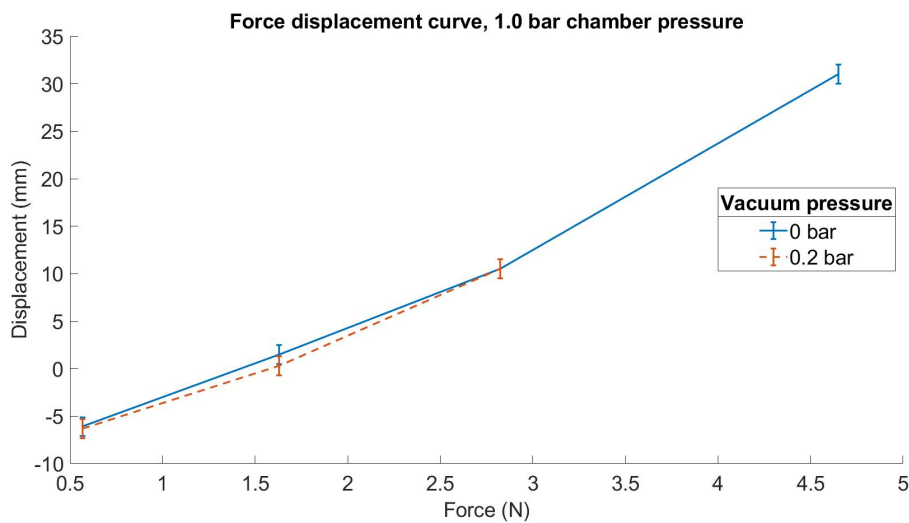


Figure 31: Force displacement curve with and without applied stiffening, for chamber pressure of 1.0 bar

### 8.3.3 Frames experiment bending back

For experiment 2 seconds after increase of pressure or other operation, a frame is saved. Figure 32 shows: from **2s** to **27s** increase of chamber pressure with steps of 0.2 bar, at **32s** actuation of the stiffening method, at **37s** release of the chambers pressure, at **47s** release of the vacuum pressure.

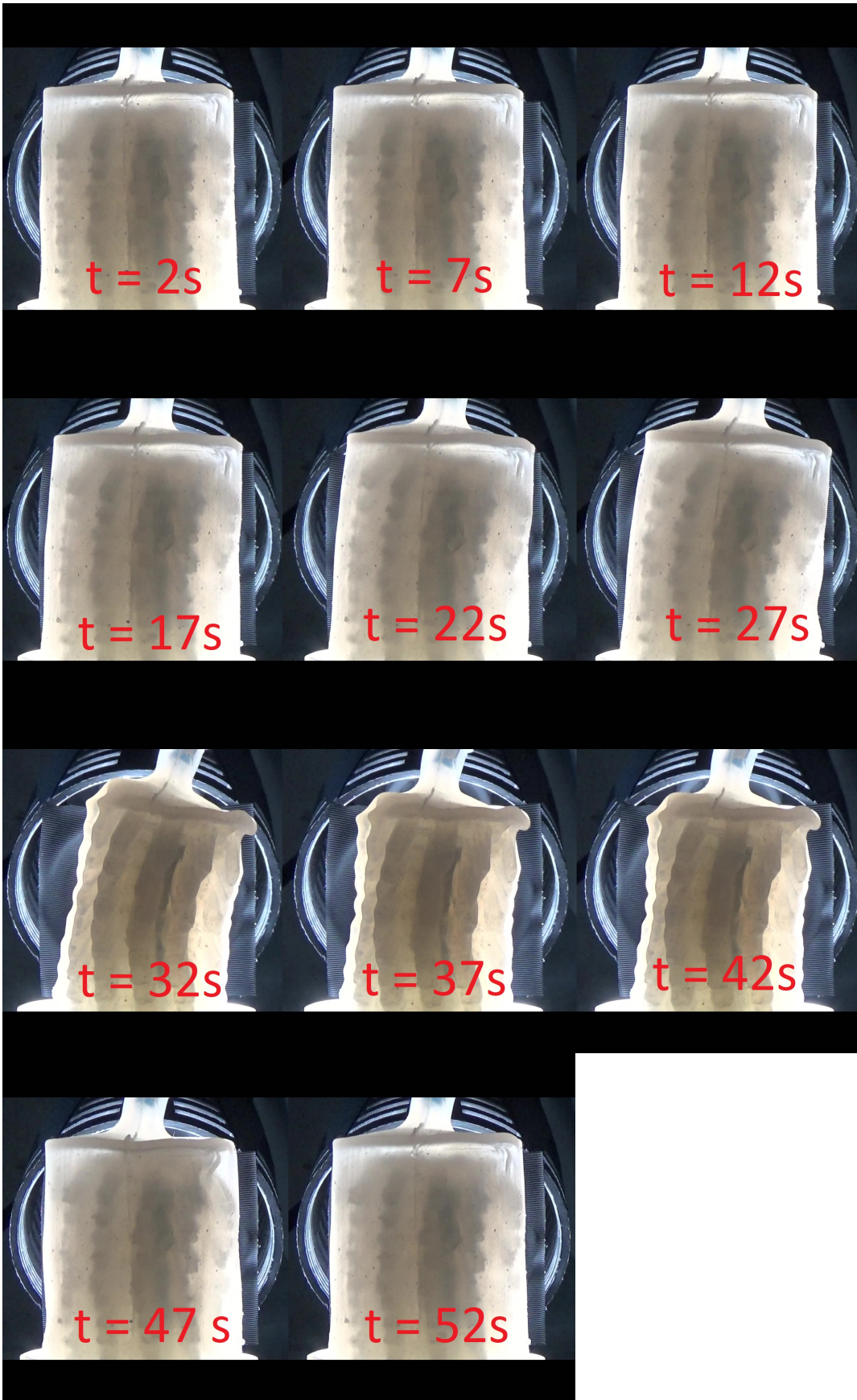


Figure 32: Frames from video of bending back experiment with 0.15 bar vacuum pressure stiffening actuation.

## References

- [1] Falco Id. soft robotics toolkit: Multi-Module Variable Stiffness Manipulator;. Available from: <https://softroboticstoolkit.com/mmvsm/design>.
- [2] Kim Y, Cheng S, Kim S, Iagnemma K. A Novel Layer Jamming Mechanism With Tunable Stiffness Capability for Minimally Invasive Surgery. *IEEE Transactions on Robotics*. 2013;29(4):1031–1042.
- [3] Hadi Sadati SM, Noh Y, Elnaz Naghibi S, Kaspar A, Nanayakkara T. Stiffness Control of Soft Robotic Manipulator for Minimally Invasive Surgery (MIS) Using Scale Jamming. In: Liu H, Kubota N, Zhu X, Dillmann R, Zhou D, editors. *Intelligent Robotics and Applications*. Cham: Springer International Publishing; 2015. p. 141–151.
- [4] Santiago JLC, Godage IS, Gonthina P, Walker ID. Soft Robots and Kangaroo Tails: Modulating Compliance in Continuum Structures Through Mechanical Layer Jamming. *Soft Robotics*. 2016 4;3(2):54–63. Available from: <https://doi.org/10.1089/soro.2015.0021>.
- [5] Blanc L, Delchambre A, Lambert P. *Flexible Medical Devices: Review of Controllable Stiffness Solutions*; 2017.
- [6] staff Bc, staff Bc. Medical gallery of Blausen Medical 2014. *WikiJournal of Medicine*. 2014;1(2):10. Available from: [https://en.wikiversity.org/wiki/WikiJournal\\_of\\_Medicine/Medical\\_gallery\\_of\\_Blausen\\_Medical\\_2014](https://en.wikiversity.org/wiki/WikiJournal_of_Medicine/Medical_gallery_of_Blausen_Medical_2014).
- [7] the digestive health centre. *Gastroscopy*;. Available from: <http://www.digestivehealth.com.au/gastroscopy/>.
- [8] Katzschmann RK, DelPreto J, MacCurdy R, Rus D. Exploration of underwater life with an acoustically controlled soft robotic fish. *Science Robotics*. 2018 3;3(16):eaar3449. Available from: <http://robotics.sciencemag.org/content/3/16/eaar3449.abstract>.
- [9] Polygerinos P, Wang Z, Galloway KC, Wood RJ, Walsh CJ. Soft robotic glove for combined assistance and at-home rehabilitation. *Robotics and Autonomous Systems*. 2015;73:135–143. Available from: <http://www.sciencedirect.com/science/article/pii/S0921889014001729>.
- [10] Cianchetti M, Ranzani T, Gerboni G, Falco ID, Laschi C, Menciassi A. STIFF-FLOP surgical manipulator: Mechanical design and experimental characterization of the single module. In: 2013 IEEE/RSJ International Conference on Intelligent Robots and Systems; 2013. p. 3576–3581.
- [11] Gifari MWM. *Study on the Design of Soft Surgical Robots for Endoscopic NOTES Applications*. University of Twente; 2018.
- [12] H Naghibi WHJWLDMMvASSMA M W Gifari. Development of a Multi-level Stiffness Soft Robotics Module with Force Haptic Feedback for Endoscopic Applications. *ICRA*. 0;.
- [13] Manti M, Cacucciolo V, Cianchetti M. Stiffening in Soft Robotics: A Review of the State of the Art. *IEEE Robotics & Automation Magazine*. 2016;23(3):93–106.
- [14] Chen Y, Li Y, Li Y, Wang Y. Stiffening of soft robotic actuators — Jamming approaches. In: 2017 IEEE International Conference on Real-time Computing and Robotics (RCAR); 2017. p. 17–21.
- [15] Cheng NG, Lobovsky MB, Keating SJ, Setapen AM, Gero KI, Hosoi AE, et al. Design and Analysis of a Robust, Low-cost, Highly Articulated manipulator enabled by jamming of granular media. In: 2012 IEEE International Conference on Robotics and Automation; 2012. p. 4328–4333.

- [16] Jiang A, Ranzani T, Gerboni G, Lekstutyte L, Althoefer K, Dasgupta P, et al. Robotic Granular Jamming: Does the Membrane Matter? *Soft Robotics*. 2014 6;1(3):192–201. Available from: <https://doi.org/10.1089/soro.2014.0002>.
- [17] Wikipedia. Electro Active Polymers;. Available from: [https://en.wikipedia.org/wiki/Electroactive\\_polymers](https://en.wikipedia.org/wiki/Electroactive_polymers).
- [18] Shian S, Bertoldi K, Clarke DR. Dielectric Elastomer Based “Grippers” for Soft Robotics. *Advanced Materials*. 2015 11;27(43):6814–6819. Available from: <https://doi.org/10.1002/adma.201503078>.
- [19] Wall V, Deimel R, Brock O. Selective stiffening of soft actuators based on jamming. In: 2015 IEEE International Conference on Robotics and Automation (ICRA); 2015. p. 252–257.
- [20] Fraś J, Czarnowski J, Maciaś M, Główska J. Static Modeling of Multisection Soft Continuum Manipulator for Stiff-Flop Project. In: Szewczyk R, Zieliński C, Kaliczyńska M, editors. *Recent Advances in Automation, Robotics and Measuring Techniques*. Cham: Springer International Publishing; 2014. p. 365–375.
- [21] Fraś J, Czarnowski J, Maciaś M, Główska J, Cianchetti M, Menciassi A. New STIFF-FLOP module construction idea for improved actuation and sensing. In: 2015 IEEE International Conference on Robotics and Automation (ICRA); 2015. p. 2901–2906.
- [22] Choi I, Corson N, Peiros L, Hawkes EW, Keller S, Follmer S. A Soft, Controllable, High Force Density Linear Brake Utilizing Layer Jamming. *IEEE Robotics and Automation Letters*. 2018;3(1):450–457.